Title:

Morphogenetic forces planar polarize LGN/Pins in the embryonic head during *Drosophila* gastrulation

Authors: Jaclyn Camuglia[1], Soline Chanet[2], Adam C Martin[1, 3]

---

[1] Biology Department, Massachusetts Institute of Technology, 77 Massachusetts Ave., Cambridge, MA 02139

[2] Center for Interdisciplinary Research in Biology, Collège de France, 11 Pl. Marcelin Berthelot, 75231 Paris

[3] Corresponding author: acmartin@mit.edu

Abstract:

Spindle orientation is often achieved by a complex of Pins/LGN, Mud/NuMa, Gαi, and Dynein, which interacts with astral microtubules to rotate the spindle. Cortical Pins/LGN recruitment serves as a critical step in this process. Here, we identify Pins-mediated planar cell polarized divisions in several of the mitotic domains of the early *Drosophila* embryo. We found that neither planar cell polarity pathways nor planar polarized myosin localization determined division orientation; instead, our findings strongly suggest that Pins planar polarity and force generated from mesoderm invagination are important. Disrupting Pins polarity via overexpression of a myristoylated version of Pins caused randomized division angles. We found that disrupting forces through chemical inhibitors, laser ablation, and depletion of an adherens junction protein disrupted Pins planar polarity and spindle orientation. Furthermore, *snail* depletion, which abrogates ventral furrow forces, disrupted Pins polarization and spindle orientation, suggesting that morphogenetic movements and resulting forces transmitted through the tissue can polarize Pins and orient division. Thus, morphogenetic forces associated with mesoderm invagination result in planar polarized Pins to mediate division orientation at a distant region of the embryo during morphogenesis. To our knowledge, this is the first *in vivo* example where mechanical force has been shown to polarize Pins to mediate division orientation.

39 **Introduction:**

40

41 Epithelial morphogenesis and homeostasis are influenced by cell division orientation, which can
42 occur along specific axes relative to both the epithelial plane and the polarity of an organ/organism
43 (Baena–Lopez et al., 2005; Kulukian and Fuchs, 2013; Lancaster and Knoblich, 2012; Morin and
44 Bellaiche, 2011). Epithelia are tissues composed of cells that are organized in a sheet and held
45 together by junctions, which maintain the integrity of the tissue as well as the apical-basal polarity
46 of cells (Choi et al., 2013; Classen et al., 2005; Cox et al., 1996; Gumbiner, 2005; Harris and
47 Peifer 2005; Tepass, 1997; Ulrich et al., 2005; Wang and Margolis, 2007). In epithelia, asymmetric
48 cell divisions, in which cellular components are distributed unequally to daughter cells, result in
49 one daughter cells leaving the epithelium. In contrast, symmetric divisions in epithelia divide
50 cellular components equally, and always result in both daughter cells remaining in the tissue.
51 Orientation of the mitotic spindle is what determines whether a division is symmetric or not, as
52 spindle orientation determines division orientation. (Cabernard and Doe, 2009; Gonczy and Rose,
53 2005; Lechler and Fuchs, 2005; Mao et al., 2011; Nakajima et al., 2013). In addition, the spindle
54 orientation with respect to organ/organism axis can promote directional growth and/or stress
55 dissipation in tissues (Campinho et al., 2013; Legoff et al., 2013; Mao et al., 2011; Mao et al.,
56 2013; Wyatt et al., 2015).

57 Spindle orientation is often achieved by a complex of Partner of Inscuteable (Pins)/LGN,
58 Mushroom Body Defect (Mud)/Nuclear Mitotic Apparatus (NuMa), Gαi, and Dynein. In this
59 complex, Pins/LGN acts as a linker between Gαi and Mud, which is also bound to a Dynein-
60 Dynactin complex. Dynein's motor activity provides the force to rotate the spindle (Bergstralh et
61 al., 2013; Busson et al., 1998; Fielmich et al., 2018; Grill and Hyman, 2005; Johnston et al., 2009;
62 Nguyen-Ngoc et al., 2007; Siller and Doe, 2008). In *Drosophila* neuroblasts, asymmetric division
63 and spindle orientation is dependent on Pins/LGN recruitment to the apical cortex. Apical proteins

64 recruit Inscuteable (Insc), which in turn recruits Pins/LGN and the spindle rotation complex. Pins
65 null mutants exhibit defects in spindle orientation in neuroblasts (Cabernard and Doe, 2009;
66 Schaefer et al., 2000; Siller et al., 2006; Yu et al., 2006). In symmetric epithelial cell divisions,
67 spindle orientation also depends on Pins, which is recruited to the lateral cortex by the lateral
68 domain protein, Discs large (Dlg). Loss of Pins, Dlg, or disrupted recruitment of Pins by Dlg causes
69 aberrant asymmetric cell divisions in epithelia and cell loss (Bell et al., 2015; Bergstralh et al.,
70 2013; Carvalho et al., 2015). Furthermore, in planar cell polarized divisions of the sensory organ
71 precursor cells in the *Drosophila* dorsal thorax, asymmetric determinant segregation and spindle
72 orientation depend on planar polarized Pins and E-cadherin localization, respectively (Bellaïche
73 et al., 2001; Le Borgne et al., 2002).

74 In addition to molecular cues, mechanical cues also orient cell division. For example, in
75 isolated cell cultures, cell division orientation has been shown to directly respond to stress by
76 aligning with applied forces (Fink et al., 2011; Matsumura et al., 2016; Thery et al., 2007; Thery
77 et al., 2005). Cells also respond to force through its influence on cell shape. The connection
78 between cell shape and division axis is known as the long axis rule or Hertwig's rule and was first
79 observed over 100 years ago (Hertwig, 1884). However, the mechanisms through which force,
80 cell shape, and molecular cues are interconnected to influence cell division remain an active area
81 of research. In epithelial tissues, cell division/spindle orientation occurs along the tension axis,
82 which can dissipate tension and influence cell packing (Campinho et al., 2013; Gibson et al.,
83 2011; Godard et al., 2020; Mao et al., 2011; Scarpa et al., 2018; Wyatt et al., 2015). In the
84 *Drosophila* pupal notum and *Xenopus,* cell shape has been shown to affect the spindle angle
85 through the influence of molecular cues localized at tri-cellular junctions, which provide a 'memory'
86 for interphase cell shape (Bosveld et al., 2016; Nestor-Bergmann et al., 2019). Whereas in the
87 *Drosophila* oocyte, follicular epithelium, and parasegmental boundaries and cultured MDCK cells,
88 molecular cues do not localize to tri-cellular junctions, implying other mechanisms are responsible
89 for force-oriented spindle rotation (Finegan et al., 2019; Gloerich et al., 2017; Scarpa et al., 2018;

90 Yu et al., 2006). For example, mechanical cues have been shown to recruit the Pins/LGN
91 machinery to adherens junctions in MDCK cells (Hart et al., 2017). Mitotic rounding forces have
92 also been shown to be important for proper spindle orientation and morphology (Chanet et al.,
93 2017; Kunda et al., 2012). The combinatorial action of mechanical and molecular cues used to
94 orient spindles is incompletely understood. Here, we use the *Drosophila* embryo as a powerful
95 model organism that is uniquely tractable, and exhibits mirror symmetric domains that undergo
96 highly stereotyped divisions to uncover the relationship between mechanical and molecular cues
97 to coordinate division orientation in a developing embryo.

98 During development the early *Drosophila* embryo undergoes thirteen cycles of
99 synchronous nuclear divisions with no intervening gap phases. After these thirteen cycles of
100 nuclear division, embryonic cells arrest in G2. Cycle 14 divisions occur in a highly stereotyped
101 pattern defined by *string* (*Drosophila* Cdc25 homologue) expression in pockets of cells across the
102 embryo. These pockets of cells that divide together are termed mitotic domains (Edgar and
103 O'Farrell, 1989; Foe, 1989). Some of these domains have been observed to have oriented
104 divisions, but the mechanism underlying division orientation is unknown (da Silva and Vincent,
105 2007; Hartenstein and Campos-Ortega, 1985; Hartenstein et al., 1987; Stern et al., 2021; Wang
106 et al., 2017). We found that spindle orientation is a highly dynamic process in which spindles are
107 not assembled oriented, but rather have to rotate to achieve orientation in mitotic domains 1, 3,
108 and 5 (MDs 1, 3, and 5) in the dorsal 'head' and are oriented in the direction of tissue
109 movement/elongation. We discovered that these oriented symmetric divisions and those of MD
110 14, which had previously been shown to exhibit force dependent oriented symmetric divisions,
111 require planar polarized Pins (da Silva and Vincent, 2007; Wang et al., 2017).
112
113
114
115

116 **Results:**

117

118 *Early mitotic domains in the Drosophila head exhibit spindle rotation and planar polarized division.*
119 Located on the dorsal side of the *Drosophila* embryo 'head', MD 1, 3, and 5 undergo division
120 during gastrulation, 200 minutes after egg deposition (AED). MD3 is the anterior most mitotic
121 domain and comprises around thirty cells, MD1 is the next most anterior domain and consists of
122 two mirrored clusters of around 40 cells, and MD5 is located just anterior to the cephalic furrow
123 and consists of two mirrored clusters containing around 30 cells (Figure 1A, B).

124 We initially visualized division axis in embryos expressing fluorescently-tagged non-
125 muscle myosin II to mark cytokinetic rings and fluorescently tagged myristoylation sequence of
126 Gap43 to mark cell membranes. Cytokinetic rings form perpendicular to the division axis. In MDs
127 1, 3, and 5, cytokinetic rings are oriented roughly perpendicular to the AP axis. (Figure 1C). To
128 further visualize the division process and assess dynamics during division, we used embryos
129 expressing fluorescently-tagged CLIP170 to mark the mitotic spindle (Figure 1D, movie 1). To
130 quantify the alignment of the divisions with the AP axis, we measured the angle between the
131 spindle and the AP axis, where an angle of 0 indicates perfect alignment with the AP axis and an
132 angle of 90 indicates alignment with the dorsal-ventral (DV) axis (Figure 1E). Spindles were
133 measured after anaphase, when spindle position becomes fixed. MDs 1, 3, and 5 divisions occur
134 almost entirely within 30° of the AP axis (Figure 1E-H).

135 Notably, we found that mitotic spindles are not initially oriented with the AP axis and form
136 with no preferential orientation. Spindles then rotate up to 90° to achieve a final orientation (Figure
137 1D). Together these data show that MDs 1, 3, and 5 exhibit oriented divisions and this orientation
138 is achieved by spindle rotation toward the AP axis. We next asked what cue(s) could coordinate
139 the spindle rotation and division orientation.

140

141 *Planar polarized divisions require polarized Pins localization*

142 Because spindles exhibited a pronounced rotation after assembly, we examined
143 components of the spindle rotation machinery, Pins and Mud. We discovered that MDs 1, 3, and
144 5 all exhibit planar cell polarity of Pins. The Pins planar cell polarity is dependent on cell cycle
145 state: mitotic cells exhibit planar polarized Pins, whereas Pins is uniformly distributed along lateral
146 membranes of interphase cells (Figure 2A, movie 2). We quantified Pins polarization by modifying
147 previously described polarization quantifications of mitotic cells (Besson et al., 2015). We used
148 embryos expressing fluorescently labelled Pins and fluorescent membrane marker
149 Gap43::mCherry, and measured the intensity of Pins::YFP and Gap43::mCherry around the
150 membrane. We found that in MD1, the Pins crescent is on the posterior side of the cells and Pins
151 intensity peaks just past the posterior-most part of the cell (Figure 2C and C'). The ratio of the
152 point of greatest Pins intensity to the average of the two adjacent troughs was greater than the
153 same ratio calculated from the Gap43::mCherry signal (peak-to-trough ratio Pins, 1.39±0.1017
154 and Gap43::mCherry, 1.04±0.0406, mean and S.D.), demonstrating that this polarity was not
155 caused by membrane inhomogeneity. Gap43::mCherry also had a more uniform labeling along
156 the membrane in MD cells (Figure 2B, D, and D'). Though our imaging resolution is not sufficient
157 to determine whether Pins is localized solely on the posterior side of MD1 cells or both the
158 posterior and anterior sides when groups of cells round up together, we find that cells on the
159 boundary of MD1 display Pins crescents only on the posterior side. Interestingly, from observation
160 of boundary cells, we find Pins is localized on the posterior side of MDs 1 and 3, but the anterior
161 side of MD5 (Figure S1).

162 In addition to MDs 1, 3, and 5 we decided to look at MD14, which has previously been
163 shown to exhibit force dependent planar polarized divisions (Wang et al., 2017). Mitotic cells
164 within MD14 exhibited planar polarized Pins, similar to what we saw for MD 1 (Figure 2H).
165 Posterior crescents of Pins form in the mitotic cells of MD 14, though the crescent is broader than

166 in MDs 1, 3, and 5. The peak to trough ratio for Pins in MD14 was different from control
167 Gap43::mCherry (1.22±0.0914 and 1.04±0.1115, respectively, mean and S.D.) (Figure 2H-K').
168 To ensure Pins polarization was not a consequence of expressing non-endogenous levels
169 of Pins, we fixed and stained embryos to localize endogenous Pins. We found that similar to
170 Pins::YFP, endogenous Pins was planar polarized in mitotic MD 1 cells (Figure 2E). We also
171 looked at components of the spindle rotation machinery complex downstream of Pins, namely
172 Mud. It appears that Mud follows a similar localization pattern as Pins and is polarized in crescents
173 in mitotic cells of MD1, although Mud also strongly labels spindle poles (Figure 2F-G). Based on
174 our live and fixed imaging, we conclude that MDs 1, 3, 5, and 14 cells exhibit planar polarized
175 Pins localization during mitosis.
176 We next sought to establish whether there was a connection between Pins polarity and
177 spindle orientation. Using embryos expressing fluorescently-tagged tubulin and fluorescently-
178 tagged Pins we monitored the timing of Pins polarization and spindle rotation. We found that Pins
179 polarization preceded spindle rotation and is abolished shortly after anaphase, when the spindle
180 position is finalized (Figure 3A-B, movie 3). The correlated timing between Pins polarization and
181 spindle rotation suggests Pins is responsible for the spindle achieving its polarized orientation. To
182 determine the relationship between Pins polarity and spindle rotation we compared the angle of
183 maximum Pins intensity to the division angle. We found that there was a strong correlation
184 between angular position of maximum Pins intensity and the anaphase spindle angle in MD 1
185 (Figure 3C). Previous studies have shown division orientation often follows the long axis of the
186 interphase cell shape (Hertwig, 1884; Minc et al., 2011; Tsou et al., 2003). To determine whether
187 division angle in the MD1 could also be related to cell shape, we compared the interphase cell
188 long-axis angle to the division angle. In contrast to Pins polarity, there was no correlation between
189 interphase cell shape and division angle, indicating the divisions of MD1 do not follow the long
190 axis rule (Figure S2). Together these data show that division orientation correlates with Pins
191 localization, but not interphase cell shape. We also analyzed Pins and tubulin within MD14, which

192 is located at the ventral midline (Figure 3D). Similar to MD 1, Pins polarization preceded spindle
193 rotation. (Figure 3E-F).

194 To test the functional requirement of Pins polarity, we analyzed spindle orientation in
195 embryos overexpressing a myristoylated Pins. Myristoylation covalently attaches a myristoyl
196 group to a protein so the protein associates with the plasma membrane in an unregulated manner.
197 Overexpression of myristoylated Pins, but not wild-type Pins, caused Pins to be uniformly
198 distributed along the membrane during mitosis and abolished Pins planar polarity (Figure S3). We
199 overexpressed the myristoylated version of Pins instead of using a Pins null mutant because we
200 and others have previously shown that the Pins null mutant causes aberrant asymmetric divisions
201 and our goal was to disrupt Pins polarity while keeping the divisions in-plane. We have previously
202 shown myristoylated Pins is functional and able to rescue off-axis divisions that occur after Dlg-
203 RNAi (Chanet et al., 2017). Despite occurring in-plane, spindles in embryos expressing
204 myristoylated Pins fail to orient along the AP axis. Instead, division angles are evenly distributed,
205 occurring with seemingly no preference between the DV and AP axes for cells within MD1 (Figure
206 3I-J, movie 4). In comparison, spindles in embryos expressing control Pins orient along the AP
207 axis, with most divisions occurring within 30° of the AP axis (Figure 3G-H). Myr-Pins expressing
208 embryos had an average division angle within MD1 that was significantly different from controls
209 (42.7 and 20.1, respectively, p=0.000103). Results for MDs 3 and 5 are consistent with MD1
210 (Figure S4A - D). Myristoylated Pins expression also disrupted division orientation in MD14. Myr-
211 Pins expressing embryos had an average division angle within MD14 that was significantly
212 different from controls (41.2 and 18.1, respectively, p=0.0079) (Figure 3K-N). These data suggest
213 that Pins polarity is necessary for mitotic spindle orientation and planar polarity of divisions within
214 MDs 1, 3, 5, and 14. Next we investigated what mechanisms establish Pins planar polarity.

215

216 *Adherens junctions, but not Toll-like receptors or other PCP pathways, are required for division*
217 *orientation.*

218 We hypothesized that Pins polarity could require an upstream planar cell polarity pathway
219 and/or a mechanical cue. We first tested the requirement of planar cell polarity pathways. Some
220 well-known planar polarity pathways include the Fat-Dachsous, the core PCP, and the PAR
221 pathways (Hale and Strutt, 2015; Strutt and Strutt, 2009). The Fat-Dachsous and core PCP
222 pathways were not good candidates from orienting divisions within MDs 1, 3, and, 5 because
223 previous work has shown the components of these pathways are not expressed early enough
224 and/or in the MDs to be involved (Clark et al., 1995; Tomancak et al., 2002; Tomancak et al.,
225 2007). The PAR pathway was also not a good candidate because the *Drosophila* homologue of
226 Par 3, Bazooka (Baz), did not exhibit planar cell polarity in the MDs, despite retaining apical
227 localization during mitosis (Ko et al., 2020). Therefore, we explored the possible involvement of
228 Toll-like receptors (TLRs), which act downstream of even-skipped (Eve) and have been shown to
229 be necessary for the planar polarity of non-muscle myosin II (Myo II) and Baz in the *Drosophila*
230 trunk (Lavalou et al., 2021; Pare et al., 2014). We investigated whether TLRs were involved in
231 division orientation by injecting live embryos with dsRNA of TLRs 2, 6, and 8 and control 0.1x TE
232 buffer. Further we analyzed fixed embryos that were triple mutants for these TLRs. These
233 perturbations did not disrupt division orientation to the extent of expressing Myr-Pins, and
234 distributions of division angles and average division angles were similar to controls (Figure S5)
235 further, Myo II and Baz were not planar polarized in the *Drosophila* head (Chanet et al., 2017; Ko
236 et al., 2020), leading us to conclude that TLRs are not solely responsible for division orientation
237 in MDs 1, 3, 5.
238 We next tested the function of AJs. AJs mechanically couple epithelia cells and are composed
239 of cadherin-catenin complexes (Hinck et al., 1994; Kovacs and Yap, 2008; Leckband and
240 Prakasam, 2006; Oda et al., 1994; Rimm et al., 1995; Takeichi, 1991; Yap et al., 1997). AJs are
241 connected to F-actin, which is required for force transmission (Nelson et al., 2005; Rauskolb et
242 al., 2014). Junctional proteins, such as Canoe/Afadin (cno), have been implicated in spindle
243 positioning (Carminati et al., 2016; Speicher et al., 2008; Wee et al., 2011). Additional work has

244 shown that E-Cadherin is able to recruit Pins in a tension dependent manner (Hart et al., 2017).
245 While AJs are not required for in-plane divisions in certain tissues (Bergstralh et al., 2013), they
246 could serve as platforms for Pins to cue division orientation. To perturb AJs, we maternally
247 depleted α-catenin (αcat) using RNAi. We have shown that αcat depletion is the most severe way
248 to disrupt adherens junctions, totally uncoupling mesoderm cell actomyosin from the junctions,
249 preventing their apical constriction, and lowering adherens junction levels throughout the entire
250 embryo (Denk-Lobnig et al., 2021; Yevick et al., 2019). We crossed the RNAi (hairpin) stock to
251 flies expressing a maternal GAL4 and fluorescently labelled tubulin to visualize spindles. When
252 compared to a control RNAi (Rh3), embryos expressing the αcat RNAi had an even distribution
253 of division angles in MD1, occurring with seemingly no preference between the DV and AP axes.
254 αcat-depleted embryos exhibited an average division angle that was significantly different from
255 controls (36.7 and 26.4, respectively; p=0.000583) (Figure 4A-D, movie 4). αcat RNAi also
256 disrupted spindle orientations in MD3 and MD5 (Figure S4E - H).
257 Because Cno has been shown to interact with Pins (Speicher et al., 2008; Wee et al., 2011),
258 we tested Cno function in MDs 1, 3, and 5. We used two RNAi lines to maternally deplete Cno
259 and crossed each to flies expressing fluorescently labelled tubulin. Measuring division angles, as
260 previously described, we found that Cno depletion does not significantly disrupt division
261 orientation within MDs 1, 3, and 5 compared to controls, Cno-depleted embryos exhibited an
262 average division angle that was not significantly different from controls (27.9 and 26.4,
263 respectively; p=0.2698) (Figure 4E – F). Note that Cno-RNAi with these lines disrupted myosin
264 localization, similarly to genetic mutants (Sawyer et al., 2011; Sawyer et al., 2009), but did not
265 fully abrogate midline convergence during ventral furrow formation (Jodoin et al., 2015), unlike
266 αcat RNAi (Denk-Lobnig et al., 2021). Together these data suggest a role for AJs and possibly
267 force transmission in spindle orientation. Given our results, we next tested whether AJs are
268 involved in polarization of Pins within MDs 1, 3, and 5.

269

270 *Disruption of adherens junction proteins disrupts Pins polarization*

271 To determine whether AJs are involved in Pins planar polarized localization, we examined
272 fluorescently labelled Pins in α-catenin-depleted embryos. In contrast to control embryos, we
273 found that Pins planar polarity is abolished when α-cat was depleted (Figure 5A-D, movie 5). Pins
274 appeared to have no preferential localization, though given that cells divide in the epithelial plane,
275 a process that depends on Pins, Pins must still localize laterally. Pins peak to trough ratio at the
276 posterior was different in controls compared to α-catenin-depleted embryos (1.33±0.0751 and
277 1.06±0.0173, respectively, mean and S.D.). These data demonstrate a role for AJs in Pins planar
278 polarization in MD 1.

279

280 *Mechanical cues affect Pins polarization and division orientation*

281 Given our results that AJs are involved in division orientation and Pins polarity and our finding
282 that Pins is planar polarized within the force dependent oriented divisions of MD14, we
283 hypothesized that force transduction through AJs contributes to Pins polarization and division
284 orientation in MDs 1, 3, and 5. To further test the role of force transmission, we injected embryos
285 expressing fluorescently labelled Pins and tubulin with a low dose of cytochalasin D (CytoD) that
286 we have shown to inhibit force transmission without globally depolymerizing F-actin (Jodoin et al.,
287 2015; Mason et al., 2013). Actomyosin is also necessary for cell rounding, which is necessary for
288 planar divisions for MD cells (Chanet et al., 2017). As we were interested in the orientation of
289 planar divisions, we focused our analysis on divisions that occurred within the plane of the
290 epithelium. We found that injections of CytoD disrupted planar polarized division orientation,
291 CytoD injected embryos exhibited an average division angle that was significantly different from
292 controls (53.7 and 21.9, respectively; p=0.0043) (Figure 6B, D, F, H). CytoD injection also
293 disrupted spindle orientations in MD3 and MD5 (Figure S4I - L). In addition, Pins polarity was

294 disrupted in embryos injected with CytoD whereas Pins is polarized in posterior crescents in
295 DMSO injected controls. The posterior Pins peak to trough ratio was different for DMSO injected
296 controls and CytoD injected embryos (1.17±0.0685 and 1.08±0.0609, respectively, mean and
297 S.D.) (Figure 6A, C, E, G, movie 5). Interestingly, injection of DMSO seems to perturb the
298 synchrony of divisions. In non-injected embryos, cells within the domain divide in a wave-like
299 pattern, starting in the middle of the domain and propagating to the domain boundary. In DMSO
300 injected embryos, nearly all cells round and divide simultaneously. This disruption in division
301 timing within the domain does not disrupt division orientation or Pins polarization. As CytoD has
302 many effects beyond disrupting forces, we next sought to test the role of tissue mechanics without
303 chemical or genetic perturbation.

304 To that end, we performed laser ablation experiments to mechanically isolate MDs from the
305 rest of the tissue. We focused on MD1 and performed a series of four cuts to isolate the domain
306 (Figure 6I). Using embryos that expressed fluorescently labelled tubulin, we analyzed the effect
307 of mechanical isolation on spindle orientation. Cells that divide within the mechanically isolated
308 region fail to orient along the AP axis (Figure 6K, N). As an internal control, we utilized the mirrored
309 spatial pattern of MD1 and cut one side of the domain and left the other side uncut (Figure 6I). In
310 the same embryo, we were able to observe spindles within the cut region fail to orient and
311 neighboring cells outside the cut region orient correctly (Figure 6J, M, movie 6). As a further
312 control, and to compensate for the difficulty in acquiring images that permitted visualization of
313 both sides of the domain, we performed sham ablations, where we irradiated the region with a
314 level of light below the cutting threshold. In sham ablated control embryos, spindles oriented with
315 preference towards the AP axis and had an average division angle that was significantly different
316 from cells within the cut region (20.0 and 58.0, respectively; p=0.0286) (Figure 6J - M).

317

318 *Mesoderm invagination polarizes Pins and division orientation in the embryonic head*

319 The divisions in MDs 1, 3, and 5 occur during gastrulation. We hypothesized that forces from
320 morphogenic events during gastrulation control Pins polarization and division orientation. We
321 focused on mesoderm invagination, which precedes divisions in MDs 1, 3, and 5 by around 10
322 minutes and pulls ectoderm cells around circumference of the embryo (Lye et al., 2015; Rauzi et
323 al., 2015). To perturb forces associated with mesoderm invagination, we decided to disrupt the
324 transcription factor Snail because Snail-depletion most severely depletes apical actomyosin
325 activity in the mesoderm (Martin et al., 2009; Mason et al., 2013). We injected Snail dsRNA into
326 embryos expressing fluorescently labelled tubulin and Pins. We found that Snail depletion
327 disrupted division orientation (Figure 7B, D, F, H, movie 7). Embryos injected with Snail dsRNA
328 had a random distribution of division angles, occurring with an average division angle significantly
329 different from controls (40.0 and 22.6, respectively; p=0.0121). In addition, Pins polarity was
330 clearly disrupted in embryos injected with Snail dsRNA. For 0.1x TE buffer injected controls, the
331 posterior Pins peak to trough ratio was different from Snail dsRNA injected embryos
332 (1.27±0.08401 and to 1.10±0.10545, respectively, mean and S.D.) (Figure 7A, C, E, G). Beyond
333 division orientation and Pins polarity, injections of Snail dsRNA disrupted the patterning of MDs
334 1, 3, and 5. Instead of three distinct domains, a single group of anterior cells divide. Taken
335 together, these data indicate morphogenic forces play a role in Pins polarity and division
336 orientation within MDs 1, 3, and 5. A role for morphogenic forces is consistent with our observation
337 that disruption of αcat or actomyosin (with CytoD) or laser ablation disrupt division orientation.
338
339 **Discussion:**
340 Here, we discovered that Pins exhibits planar cell polarity in mitotic domains of the dorsal
341 head (MDs 1, 3, and 5) and along the ventral midline (MD14). We demonstrated that Pins polarity
342 is required for spindle orientation by overexpressing a myristoylated version of Pins that exhibits
343 unregulated cortical localization and disrupts spindle orientation. Furthermore, we found that Pins
344 planar cell polarity and AP spindle orientation depend on adherens junctions. Finally, we showed

345 that disrupting mesoderm invagination, disrupting actomyosin, or disconnecting MD cells from
346 surrounding tissue by laser ablation disrupted Pins polarization and spindle orientation,
347 suggesting that morphogenetic movements and resulting forces transmitted through the tissue
348 can polarize Pins.
349
350 *Other mechanisms of division orientation*
351 Several other mechanisms of planar polarized division orientation have been identified.
352 Previous works have shown that planar cell polarity pathways, namely the Fat/Dachsous, the core
353 PCP and the PAR pathways, coordinate divisions of the fly wing disc, during Zebrafish
354 gastrulation, and in *Drosophila* sensory organ precursor (SOP) cells, amongst other contexts
355 (Baena-Lopez et al., 2005; Besson et al., 2015; Concha and Adams, 1998; Gho and Schweisguth,
356 1998; Gong et al., 2004; Mao et al., 2006). We ruled out the Fat/Dachsous and core PCP
357 pathways because previous studies indicated the components of these pathways are not
358 expressed early enough in development to play a role in orienting the divisions of the dorsal head
359 or ventral midline (Clark et al., 1995; Tomancak et al., 2002; Tomancak et al., 2007). We further
360 confirmed this by examining fluorescently tagged versions of proteins within these pathways. As
361 was reported, we found no evidence of appreciable expression of these proteins (data not shown).
362 Further, we ruled out the PAR pathway because we saw no evidence of planar polarity in
363 Bazooka/Par 3 (Ko et al., 2020). The Toll-like receptor planar polarity pathway identified in the
364 *Drosophila* trunk was a candidate for involvement in the mitotic domains (Pare et al., 2014). We
365 ruled out this pathway for two reasons, first the TLR pathway in the *Drosophila* trunk results in
366 polarized Myosin and Bazooka/Par3. Observation of these proteins in the dorsal head showed no
367 strong polarization of either protein (Chanet et al., 2017; Ko et al., 2020). Second, we generated
368 a triple mutant of the TLRs identified and performed injections of dsRNA of these TLRs. In each
369 case, spindle orientation was not affected to the extent of the myristoylated Pins perturbation.
370 Indicating TLRs cannot be solely responsible for spindle orientation in MDs 1, 3, and 5.

371 Hertwig's rule or the long axis rule is perhaps the most established mechanism of division
372 orientation. More recent studies have shown that tricellular junctions are a better predictor of
373 division orientation than the long axis. Mud localizes to tricellular junctions which cues spindle
374 orientation (Bosveld et al., 2016). We did not observe Mud localization to tricellular junctions within
375 the dorsal head mitotic domains and along the ventral midline. Further, we find no correlation
376 between cell long axis and division orientation within these domains.
377
378 *Myosin-dependent tension and division orientation*
379 Myosin-dependent tension has been shown to cue the orientation of the mitotic spindle. A
380 growing body of work suggests a role for tension in division orientation, with notable examples in
381 fly development. In the fly notum, it was shown that cells rely on isotropic myosin-dependent
382 tension to sense cell shape and divide along the cell long axis (Lam et al., 2020). Unlike the cells
383 of the fly notum, cells within MDs 1, 3, 5, and 14 do not follow the long axis rule. However, isotropic
384 myosin-dependent tension is required for cell rounding and for symmetric cell divisions in MD
385 cells (Chanet et al., 2017).
386 Tension has also been shown to overrule the long axis rule and orient divisions with the
387 axis of tension rather than the cell long axis. In the follicular epithelium, cortical tension at the
388 apical surface cues planar divisions in a Canoe dependent manner. Pins and Mud were not planar
389 polarized but rather localized around the entire cell cortex and did not play a role in the planar
390 divisions within the follicular epithelium (Finegan et al., 2019). Similarly, in parasegmental
391 boundaries, local anisotropy in myosin-dependent tension overrides cell shape. In this context it
392 was shown that tension is both necessary and sufficient to cue division orientation. Pins and Mud
393 were shown to not be involved in division orientation but were necessary for planar divisions.
394 (Scarpa et al., 2018). In the mitotic domains, we did not observe anisotropic myosin-dependent
395 tension. Instead, we observe a uniform distribution of actin and myosin within the dorsal head.

396 While myosin-dependent tension plays an important role in division orientation in different context
397 within fly development, we found no evidence of a role in the oriented divisions of the dorsal head.
398
399 *Adherens junctions and division orientation*
400 Prior work suggested that adherens junctions are involved in division orientation. Notably,
401 within *Drosophila* male germline stem cells (Inaba et al., 2010) and sensory organ precursor cells
402 (Le Borgne et al., 2002) the adherens junction component, E-cadherin is localized asymmetrically
403 and coordinates the asymmetric divisions within these cells. Perturbation of E-cadherin results in
404 misorientation of the mitotic spindle. Interestingly, in sensory organ precursor cells it was also
405 shown that perturbation of E-cadherin disrupted the localization of Pins, although Pins still
406 appears as a crescent (Le Borgne et al., 2002).
407 E-cadherin also has a demonstrated role in symmetric divisions. In MDCK cells E-cadherin
408 recruits Pins in a tension-dependent manner. It was previously known that Pins/LGN localizes to
409 junctions, but this study first showed a role for force in Pins' junctional localization (Hart et al.,
410 2017). Our findings are consistent with these results. As seen in the MDCK cells, in cells within
411 the dorsal head mitotic domains and ventral midline adherens junctions may sense anisotropic
412 force within the tissue and recruit spindle rotation machinery in a polarized fashion to cue division
413 orientation. To our knowledge, this is the first *in vivo* example where mechanical force has been
414 shown to polarize Pins to mediate division orientation.
415
416 *Role of divisions in morphogenesis*
417 An important question that remains is the function of the oriented divisions of the dorsal
418 head during morphogenesis. The oriented divisions of the ventral midline (MD14) have been
419 shown to alleviate tissue strain and promote tissue elongation by promoting an increase in surface
420 area of the mesectoderm (Wang et al., 2017). This agrees with other studies which suggest that
421 oriented division facilitate tissue elongation during development (Aigouy et al., 2010; Baena–

422 Lopez et al., 2005; Gong et al., 2004; Mao et al., 2011). A recent study expanded on the role of
423 divisions during gastrulation. By following all the cell intercalations, movements, and divisions
424 during gastrulation, the authors show cell divisions compensate for the cell loss due to various
425 invaginations (Stern et al., 2021). Indeed, past work has shown that cell division can lead to
426 oriented pushing forces that could contribute to morphogenesis (Gupta et al., 2021). In the
427 embryo, apical relaxation that results from mitotic entry and the following oriented division has
428 been shown to give rise to ectopic tissue folds (Ko et al., 2020). Therefore, we speculate that the
429 oriented division of the dorsal head facilitate tissue elongation and compensate for cell loss from
430 mesoderm and cephalic furrow invagination.
431
432 *Study limitations and future directions*
433 While the evidence in this study supports the hypothesis that morphogenic forces polarize
434 Pins which is required for division orientation, the interpretation of this evidence is limited by
435 certain aspects of the study. First, in describing Pins crescents in mitotic cells, we argue that Pins
436 is on the posterior side for MDs 1 and 3 and anterior side for MD5 (Figure 2A, C, movie 2, Figure
437 S1). This result is based on observation of cells on the boundary of mitotic domains that are not
438 surrounded by other mitotic cells. We do not have the resolution to determine whether Pins is on
439 one or both sides of cells within the domains. One question that arises from this observation is:
440 how does a junction that is under tension recruit Pins to just one side? It is of interest to understand
441 the sidedness of Pins in the mitotic domains and what causes this sidedness.
442 More broadly, it is of interest to understand how Pins is specifically recruited along the AP
443 axis. While we show that disruption of mesoderm invagination is necessary for division orientation,
444 what provides the directionality of the divisions remains unknown. Previous work has shown
445 tissue flows that correspond to the division orientations we observe (Streichan et al., 2018). More
446 work is needed to determine how forces generated at the ventral midline orient divisions in the
447 dorsal head.

448 Finally, we can only speculate on the significance of these oriented divisions during
449 morphogenesis. Planar, oriented division have been shown to be involved in tissue elongation
450 and folding (Baena–Lopez et al., 2005; Kulukian and Fuchs, 2013; Lancaster and Knoblich, 2012;
451 Morin and Bellaiche, 2011). Given that the divisions of MDs 1, 3, 5, and 14 take place during
452 gastrulation, we hypothesize that the divisions may aid in morphogenic movements such as germ-
453 band extension and cephalic furrow invagination, but we have not directly tested this. These
454 questions form the basis of future work into the relationship between mechanical and molecular
455 cues in division orientation and the contribution of division orientation during development.
456
457
458
459
460
461
462
463
464
465
466
467
468
469
470
471
472
473

474 **References**

475 Aigouy, B., R. Farhadifar, D.B. Staple, A. Sagner, J.C. Roper, F. Julicher, and S. Eaton. 2010. Cell
476 flow reorients the axis of planar polarity in the wing epithelium of Drosophila. *Cell*.
477 142:773-786.
478 Baena-Lopez, L.A., A. Baonza, and A. Garcia-Bellido. 2005. The orientation of cell divisions
479 determines the shape of Drosophila organs. *Curr Biol*. 15:1640-1644.
480 Bell, G.P., G.C. Fletcher, R. Brain, and B.J. Thompson. 2015. Aurora kinases phosphorylate Lgl to
481 induce mitotic spindle orientation in Drosophila epithelia. *Curr Biol*. 25:61-68.
482 Bellaïche, Y., A. Radovic, D.F. Woods, C.D. Hough, M.L. Parmentier, C.J. O'Kane, P.J. Bryant, and
483 F. Schweisguth. 2001. The Partner of Inscuteable/Discs-large complex is required to
484 establish planar polarity during asymmetric cell division in Drosophila. *Cell*. 106:355-366.
485 Bergstralh, D.T., H.E. Lovegrove, and D. St Johnston. 2013. Discs large links spindle orientation
486 to apical-basal polarity in Drosophila epithelia. *Curr Biol*. 23:1707-1712.
487 Besson, C., F. Bernard, F. Corson, H. Rouault, E. Reynaud, A. Keder, K. Mazouni, and F.
488 Schweisguth. 2015. Planar Cell Polarity Breaks the Symmetry of PAR Protein Distribution
489 prior to Mitosis in Drosophila Sensory Organ Precursor Cells. *Curr Biol*. 25:1104-1110.
490 Bosveld, F., O. Markova, B. Guirao, C. Martin, Z. Wang, A. Pierre, M. Balakireva, I. Gaugue, A.
491 Ainslie, N. Christophorou, D.K. Lubensky, N. Minc, and Y. Bellaiche. 2016. Epithelial
492 tricellular junctions act as interphase cell shape sensors to orient mitosis. *Nature*.
493 530:495-498.
494 Busson, S., D. Dujardin, A. Moreau, J. Dompierre, and J.R. De Mey. 1998. Dynein and dynactin
495 are localized to astral microtubules and at cortical sites in mitotic epithelial cells. *Curr*
496 *Biol*. 8:541-544.
497 Cabernard, C., and C.Q. Doe. 2009. Apical/basal spindle orientation is required for neuroblast
498 homeostasis and neuronal differentiation in Drosophila. *Dev Cell*. 17:134-141.
499 Campinho, P., M. Behrndt, J. Ranft, T. Risler, N. Minc, and C.P. Heisenberg. 2013. Tension-
500 oriented cell divisions limit anisotropic tissue tension in epithelial spreading during
501 zebrafish epiboly. *Nat Cell Biol*. 15:1405-1414.
502 Carminati, M., S. Gallini, L. Pirovano, A. Alfieri, S. Bisi, and M. Mapelli. 2016. Concomitant
503 binding of Afadin to LGN and F-actin directs planar spindle orientation. *Nat Struct Mol*
504 *Biol*. 23:155-163.
505 Carvalho, C.A., S. Moreira, G. Ventura, C.E. Sunkel, and E. Morais-de-Sá. 2015. Aurora A triggers
506 Lgl cortical release during symmetric division to control planar spindle orientation. *Curr*
507 *Biol*. 25:53-60.
508 Chanet, S., R. Sharan, Z. Khan, and A.C. Martin. 2017. Myosin 2-Induced Mitotic Rounding
509 Enables Columnar Epithelial Cells to Interpret Cortical Spindle Positioning Cues. *Curr*
510 *Biol*. 27:3350-3358 e3353.
511 Choi, W., N.J. Harris, K.D. Sumigray, and M. Peifer. 2013. Rap1 and Canoe/afadin are essential
512 for establishment of apical-basal polarity in the Drosophila embryo. *Mol Biol Cell*.
513 24:945-963.
514 Clark, H.F., D. Brentrup, K. Schneitz, A. Bieber, C. Goodman, and M. Noll. 1995. Dachsous
515 encodes a member of the cadherin superfamily that controls imaginal disc
516 morphogenesis in Drosophila. *Genes Dev*. 9:1530-1542.

517 Classen, A.K., K.I. Anderson, E. Marois, and S. Eaton. 2005. Hexagonal packing of Drosophila
518 wing epithelial cells by the planar cell polarity pathway. *Dev Cell*. 9:805-817.
519 Concha, M.L., and R.J. Adams. 1998. Oriented cell divisions and cellular morphogenesis in the
520 zebrafish gastrula and neurula: a time-lapse analysis. *Development*. 125:983-994.
521 Cox, R.T., C. Kirkpatrick, and M. Peifer. 1996. Armadillo is required for adherens junction
522 assembly, cell polarity, and morphogenesis during Drosophila embryogenesis. *Journal of*
523 *Cell Biology*. 134:133-148.
524 da Silva, S.M., and J.P. Vincent. 2007. Oriented cell divisions in the extending germband of
525 Drosophila. *Development*. 134:3049-3054.
526 Denk-Lobnig, M., J.F. Totz, N.C. Heer, J. Dunkel, and A.C. Martin. 2021. Combinatorial patterns
527 of graded RhoA activation and uniform F-actin depletion promote tissue curvature.
528 *Development*. 148.
529 Edgar, B.A., and P.H. O'Farrell. 1989. Genetic control of cell division patterns in the Drosophila
530 embryo. *Cell*. 57:177-187.
531 Fielmich, L.E., R. Schmidt, D.J. Dickinson, B. Goldstein, A. Akhmanova, and S. van den Heuvel.
532 2018. Optogenetic dissection of mitotic spindle positioning in vivo. *Elife*. 7.
533 Finegan, T.M., D. Na, C. Cammarota, A.V. Skeeters, T.J. Nadasi, N.S. Dawney, A.G. Fletcher, P.W.
534 Oakes, and D.T. Bergstralh. 2019. Tissue tension and not interphase cell shape
535 determines cell division orientation in the Drosophila follicular epithelium. *EMBO J*. 38.
536 Fink, J., N. Carpi, T. Betz, A. Betard, M. Chebah, A. Azioune, M. Bornens, C. Sykes, L. Fetler, D.
537 Cuvelier, and M. Piel. 2011. External forces control mitotic spindle positioning. *Nat Cell*
538 *Biol*. 13:771-778.
539 Foe, V.E. 1989. Mitotic domains reveal early commitment of cells in Drosophila embryos.
540 *Development*. 107:1-22.
541 Gho, M., and F. Schweisguth. 1998. Frizzled signalling controls orientation of asymmetric sense
542 organ precursor cell divisions in Drosophila. *Nature*. 393:178-181.
543 Gibson, W.T., J.H. Veldhuis, B. Rubinstein, H.N. Cartwright, N. Perrimon, G.W. Brodland, R.
544 Nagpal, and M.C. Gibson. 2011. Control of the mitotic cleavage plane by local epithelial
545 topology. *Cell*. 144:427-438.
546 Gloerich, M., J.M. Bianchini, K.A. Siemers, D.J. Cohen, and W.J. Nelson. 2017. Cell division
547 orientation is coupled to cell-cell adhesion by the E-cadherin/LGN complex. *Nat*
548 *Commun*. 8:13996.
549 Godard, B.G., R. Dumollard, E. Munro, J. Chenevert, C. Hebras, A. McDougall, and C.P.
550 Heisenberg. 2020. Apical Relaxation during Mitotic Rounding Promotes Tension-
551 Oriented Cell Division. *Dev Cell*. 55:695-706 e694.
552 Gonczy, P., and L.S. Rose. 2005. Asymmetric cell division and axis formation in the embryo.
553 *WormBook*:1-20.
554 Gong, Y., C. Mo, and S.E. Fraser. 2004. Planar cell polarity signalling controls cell division
555 orientation during zebrafish gastrulation. *Nature*. 430:689-693.
556 Grill, S.W., and A.A. Hyman. 2005. Spindle positioning by cortical pulling forces. *Dev Cell*. 8:461-
557 465.
558 Gumbiner, B.M. 2005. Regulation of cadherin-mediated adhesion in morphogenesis. *Nat Rev*
559 *Mol Cell Biol*. 6:622-634.

560 Gupta, V.K., S. Nam, D. Yim, J. Camuglia, J.L. Martin, E.N. Sanders, L.E. O'Brien, A.C. Martin, T.
561 Kim, and O. Chaudhuri. 2021. The nature of cell division forces in epithelial monolayers.
562 *J Cell Biol*. 220.
563 Hale, R., and D. Strutt. 2015. Conservation of Planar Polarity Pathway Function Across the
564 Animal Kingdom. *Annual Review of Genetics*. 49:529-551.
565 Harris , T.J.C., and M. Peifer 2005. The positioning and segregation of apical cues during
566 epithelial polarity establishment in Drosophila. *Journal of Cell Biology*. 170:813-823.
567 Hart, K.C., J. Tan, K.A. Siemers, J.Y. Sim, B.L. Pruitt, W.J. Nelson, and M. Gloerich. 2017. E-
568 cadherin and LGN align epithelial cell divisions with tissue tension independently of cell
569 shape. *Proc Natl Acad Sci U S A*. 114:E5845-E5853.
570 Hartenstein, V., and J.A. Campos-Ortega. 1985. Fate-mapping in wild-typeDrosophila
571 melanogaster. *Wilhelm Roux's archives of developmental biology*. 194:181-195.
572 Hartenstein, V., E. Rudloff, and J.A. Campos-Ortega. 1987. The pattern of proliferation of the
573 neuroblasts in the wild-type embryo of Drosophila melanogaster. *Rouxs Arch Dev Biol*.
574 196:473-485.
575 Hertwig, O. 1884. Das Problem der Befruchtung und der Isotropie des Eies, eine Theorie der
576 Vererbung, Jena.
577 Hinck, L., I.S. Näthke, J. Papkoff, and W.J. Nelson. 1994. Dynamics of cadherin/catenin complex
578 formation: novel protein interactions and pathways of complex assembly. *J Cell Biol*.
579 125:1327-1340.
580 Inaba, M., H. Yuan, V. Salzmann, M.T. Fuller, and Y.M. Yamashita. 2010. E-cadherin is required
581 for centrosome and spindle orientation in Drosophila male germline stem cells. *PLoS*
582 *One*. 5:e12473.
583 Jodoin, J.N., J.S. Coravos, S. Chanet, C.G. Vasquez, M. Tworoger, E.R. Kingston, L.A. Perkins, N.
584 Perrimon, and A.C. Martin. 2015. Stable Force Balance between Epithelial Cells Arises
585 from F-Actin Turnover. *Dev Cell*. 35:685-697.
586 Johnston, C.A., K. Hirono, K.E. Prehoda, and C.Q. Doe. 2009. Identification of an Aurora-
587 A/PinsLINKER/Dlg spindle orientation pathway using induced cell polarity in S2 cells.
588 *Cell*. 138:1150-1163.
589 Ko, C.S., P. Kalakuntla, and A.C. Martin. 2020. Apical Constriction Reversal upon Mitotic Entry
590 Underlies Different Morphogenetic Outcomes of Cell Division. *Mol Biol Cell*. 31:1663-
591 1674.
592 Kovacs, E.M., and A.S. Yap. 2008. Cell-cell contact: cooperating clusters of actin and cadherin.
593 *Curr Biol*. 18:R667-r669.
594 Kulukian, A., and E. Fuchs. 2013. Spindle orientation and epidermal morphogenesis. *Philos*
595 *Trans R Soc Lond B Biol Sci*. 368:20130016.
596 Kunda, P., N.T. Rodrigues, E. Moeendarbary, T. Liu, A. Ivetic, G. Charras, and B. Baum. 2012.
597 PP1-mediated moesin dephosphorylation couples polar relaxation to mitotic exit. *Curr*
598 *Biol*. 22:231-236.
599 Lam, M.S.Y., A. Lisica, N. Ramkumar, G. Hunter, Y. Mao, G. Charras, and B. Baum. 2020.
600 Isotropic myosin-generated tissue tension is required for the dynamic orientation of the
601 mitotic spindle. *Mol Biol Cell*. 31:1370-1379.
602 Lancaster, M.A., and J.A. Knoblich. 2012. Spindle orientation in mammalian cerebral cortical
603 development. *Curr Opin Neurobiol*. 22:737-746.

604 Lavalou, J., Q. Mao, S. Harmansa, S. Kerridge, A.C. Lellouch, J.M. Philippe, S. Audebert, L.
605 Camoin, and T. Lecuit. 2021. Formation of polarized contractile interfaces by self-
606 organized Toll-8/Cirl GPCR asymmetry. *Dev Cell*. 56:1574-1588 e1577.
607 Le Borgne, R., Y. Bellaiche, and F. Schweisguth. 2002. Drosophila E-cadherin regulates the
608 orientation of asymmetric cell division in the sensory organ lineage. *Curr Biol*. 12:95-104.
609 Lechler, T., and E. Fuchs. 2005. Asymmetric cell divisions promote stratification and
610 differentiation of mammalian skin. *Nature*. 437:275-280.
611 Leckband, D., and A. Prakasam. 2006. Mechanism and dynamics of cadherin adhesion. *Annu*
612 *Rev Biomed Eng*. 8:259-287.
613 Legoff, L., H. Rouault, and T. Lecuit. 2013. A global pattern of mechanical stress polarizes cell
614 divisions and cell shape in the growing Drosophila wing disc. *Development*. 140:4051-
615 4059.
616 Lye, C.M., G.B. Blanchard, H.W. Naylor, L. Muresan, J. Huisken, R.J. Adams, and B. Sanson. 2015.
617 Mechanical Coupling between Endoderm Invagination and Axis Extension in Drosophila.
618 *PLoS Biol*. 13:e1002292.
619 Mao, Y., C. Rauskolb, E. Cho, W.L. Hu, H. Hayter, G. Minihan, F.N. Katz, and K.D. Irvine. 2006.
620 Dachs: an unconventional myosin that functions downstream of Fat to regulate growth,
621 affinity and gene expression in Drosophila. *Development*. 133:2539-2551.
622 Mao, Y., A.L. Tournier, P.A. Bates, J.E. Gale, N. Tapon, and B.J. Thompson. 2011. Planar
623 polarization of the atypical myosin Dachs orients cell divisions in Drosophila. *Genes Dev*.
624 25:131-136.
625 Mao, Y., A.L. Tournier, A. Hoppe, L. Kester, B.J. Thompson, and N. Tapon. 2013. Differential
626 proliferation rates generate patterns of mechanical tension that orient tissue growth.
627 *EMBO J*. 32:2790-2803.
628 Martin, A.C., M. Kaschube, and E.F. Wieschaus. 2009. Pulsed contractions of an actin–myosin
629 network drive apical constriction. *Nature*. 457:495-499.
630 Mason, F.M., M. Tworoger, and A.C. Martin. 2013. Apical domain polarization localizes actin-
631 myosin activity to drive ratchet-like apical constriction. *Nat Cell Biol*. 15:926-936.
632 Matsumura, S., T. Kojidani, Y. Kamioka, S. Uchida, T. Haraguchi, A. Kimura, and F. Toyoshima.
633 2016. Interphase adhesion geometry is transmitted to an internal regulator for spindle
634 orientation via caveolin-1. *Nat Commun*. 7:ncomms11858.
635 Minc, N., D. Burgess, and F. Chang. 2011. Influence of cell geometry on division-plane
636 positioning. *Cell*. 144:414-426.
637 Morin, X., and Y. Bellaiche. 2011. Mitotic spindle orientation in asymmetric and symmetric cell
638 divisions during animal development. *Dev Cell*. 21:102-119.
639 Nakajima, Y., E.J. Meyer, A. Kroesen, S.A. McKinney, and M.C. Gibson. 2013. Epithelial junctions
640 maintain tissue architecture by directing planar spindle orientation. *Nature*. 500:359-
641 362.
642 Nelson, C.M., R.P. Jean, J.L. Tan, W.F. Liu, N.J. Sniadecki, A.A. Spector, and C.S. Chen. 2005.
643 Emergent patterns of growth controlled by multicellular form and mechanics.
644 *Proceedings of the National Academy of Sciences of the United States of America*.
645 102:11594-11599.

646 Nestor-Bergmann, A., G.A. Stooke-Vaughan, G.K. Goddard, T. Starborg, O.E. Jensen, and S.
647 Woolner. 2019. Decoupling the Roles of Cell Shape and Mechanical Stress in Orienting
648 and Cueing Epithelial Mitosis. *Cell Rep*. 26:2088-2100 e2084.
649 Nguyen-Ngoc, T., K. Afshar, and P. Gonczy. 2007. Coupling of cortical dynein and G alpha
650 proteins mediates spindle positioning in Caenorhabditis elegans. *Nat Cell Biol*. 9:1294-
651 1302.
652 Oda, H., T. Uemura, Y. Harada, Y. Iwai, and M. Takeichi. 1994. A Drosophila homolog of cadherin
653 associated with armadillo and essential for embryonic cell-cell adhesion. *Dev Biol*.
654 165:716-726.
655 Pare, A.C., A. Vichas, C.T. Fincher, Z. Mirman, D.L. Farrell, A. Mainieri, and J.A. Zallen. 2014. A
656 positional Toll receptor code directs convergent extension in Drosophila. *Nature*.
657 515:523-527.
658 Rauskolb, C., S. Sun, G. Sun, Y. Pan, and K.D. Irvine. 2014. Cytoskeletal tension inhibits Hippo
659 signaling through an Ajuba-Warts complex. *Cell*. 158:143-156.
660 Rauzi, M., U. Krzic, T.E. Saunders, M. Krajnc, P. Ziherl, L. Hufnagel, and M. Leptin. 2015. Embryo-
661 scale tissue mechanics during Drosophila gastrulation movements. *Nature*
662 *Communications*. 6:8677.
663 Rimm, D.L., E.R. Koslov, P. Kebriaei, C.D. Cianci, and J.S. Morrow. 1995. Alpha 1(E)-catenin is an
664 actin-binding and -bundling protein mediating the attachment of F-actin to the
665 membrane adhesion complex. *Proceedings of the National Academy of Sciences of the*
666 *United States of America*. 92:8813-8817.
667 Sawyer, J.K., W. Choi, K.C. Jung, L. He, N.J. Harris, and M. Peifer. 2011. A contractile actomyosin
668 network linked to adherens junctions by Canoe/afadin helps drive convergent
669 extension. *Mol Biol Cell*. 22:2491-2508.
670 Sawyer, J.K., N.J. Harris, K.C. Slep, U. Gaul, and M. Peifer. 2009. The Drosophila afadin
671 homologue Canoe regulates linkage of the actin cytoskeleton to adherens junctions
672 during apical constriction. *J Cell Biol*. 186:57-73.
673 Scarpa, E., C. Finet, G.B. Blanchard, and B. Sanson. 2018. Actomyosin-Driven Tension at
674 Compartmental Boundaries Orients Cell Division Independently of Cell Geometry In
675 Vivo. *Dev Cell*. 47:727-740 e726.
676 Schaefer, M., A. Shevchenko, A. Shevchenko, and J.A. Knoblich. 2000. A protein complex
677 containing Inscuteable and the Galpha-binding protein Pins orients asymmetric cell
678 divisions in Drosophila. *Curr Biol*. 10:353-362.
679 Siller, K.H., C. Cabernard, and C.Q. Doe. 2006. The NuMA-related Mud protein binds Pins and
680 regulates spindle orientation in Drosophila neuroblasts. *Nat Cell Biol*. 8:594-600.
681 Siller, K.H., and C.Q. Doe. 2008. Lis1/dynactin regulates metaphase spindle orientation in
682 Drosophila neuroblasts. *Dev Biol*. 319:1-9.
683 Speicher, S., A. Fischer, J. Knoblich, and A. Carmena. 2008. The PDZ protein Canoe regulates the
684 asymmetric division of Drosophila neuroblasts and muscle progenitors. *Curr Biol*.
685 18:831-837.
686 Stern, T., S.J. Streichan, S.Y. Shvartsman, and E.F. Wieschaus. 2021. Deconstructing Gastrulation
687 at the Single Cell Level. *bioRxiv*:2021.2009.2016.460711.

688 Streichan, S.J., M.F. Lefebvre, N. Noll, E.F. Wieschaus, and B.I. Shraiman. 2018. Global
689 morphogenetic flow is accurately predicted by the spatial distribution of myosin motors.
690 *Elife*. 7.
691 Strutt, H., and D. Strutt. 2009. Asymmetric localisation of planar polarity proteins: Mechanisms
692 and consequences. *Semin Cell Dev Biol*. 20:957-963.
693 Takeichi, M. 1991. Cadherin cell adhesion receptors as a morphogenetic regulator. *Science*.
694 251:1451-1455.
695 Tepass, U. 1997. Epithelial differentiation in Drosophila. *Bioessays*. 19:673-682.
696 Thery, M., A. Jimenez-Dalmaroni, V. Racine, M. Bornens, and F. Julicher. 2007. Experimental
697 and theoretical study of mitotic spindle orientation. *Nature*. 447:493-496.
698 Thery, M., V. Racine, A. Pepin, M. Piel, Y. Chen, J.B. Sibarita, and M. Bornens. 2005. The
699 extracellular matrix guides the orientation of the cell division axis. *Nat Cell Biol*. 7:947-
700 953.
701 Tomancak, P., A. Beaton, R. Weiszmann, E. Kwan, S. Shu, S.E. Lewis, S. Richards, M. Ashburner,
702 V. Hartenstein, S.E. Celniker, and G.M. Rubin. 2002. Systematic determination of
703 patterns of gene expression during Drosophila embryogenesis. *Genome Biol*.
704 3:Research0088.
705 Tomancak, P., B.P. Berman, A. Beaton, R. Weiszmann, E. Kwan, V. Hartenstein, S.E. Celniker,
706 and G.M. Rubin. 2007. Global analysis of patterns of gene expression during Drosophila
707 embryogenesis. *Genome Biol*. 8:R145.
708 Tsou, M.F., W. Ku, A. Hayashi, and L.S. Rose. 2003. PAR-dependent and geometry-dependent
709 mechanisms of spindle positioning. *J Cell Biol*. 160:845-855.
710 Ulrich, F., M. Krieg, E.M. Schotz, V. Link, I. Castanon, V. Schnabel, A. Taubenberger, D. Mueller,
711 P.H. Puech, and C.P. Heisenberg. 2005. Wnt11 functions in gastrulation by controlling
712 cell cohesion through Rab5c and E-cadherin. *Dev Cell*. 9:555-564.
713 Wang, M.F., M.V. Hunter, G. Wang, C. McFaul, C.M. Yip, and R. Fernandez-Gonzalez. 2017.
714 Automated cell tracking identifies mechanically oriented cell divisions during Drosophila
715 axis elongation. *Development*. 144:1350-1361.
716 Wang, Q., and B. Margolis. 2007. Apical junctional complexes and cell polarity. *Kidney Int*.
717 72:1448-1458.
718 Wee, B., C.A. Johnston, K.E. Prehoda, and C.Q. Doe. 2011. Canoe binds RanGTP to promote
719 Pins(TPR)/Mud-mediated spindle orientation. *J Cell Biol*. 195:369-376.
720 Wyatt, T.P., A.R. Harris, M. Lam, Q. Cheng, J. Bellis, A. Dimitracopoulos, A.J. Kabla, G.T. Charras,
721 and B. Baum. 2015. Emergence of homeostatic epithelial packing and stress dissipation
722 through divisions oriented along the long cell axis. *Proc Natl Acad Sci U S A*. 112:5726-
723 5731.
724 Yap, A.S., W.M. Brieher, and B.M. Gumbiner. 1997. Molecular and functional analysis of
725 cadherin-based adherens junctions. *Annu Rev Cell Dev Biol*. 13:119-146.
726 Yevick, H.G., P.W. Miller, J. Dunkel, and A.C. Martin. 2019. Structural Redundancy in
727 Supracellular Actomyosin Networks Enables Robust Tissue Folding. *Dev Cell*. 50:586-598
728 e583.
729 Yu, F., C.T. Kuo, and Y.N. Jan. 2006. Drosophila neuroblast asymmetric cell division: recent
730 advances and implications for stem cell biology. *Neuron*. 51:13-20.
731

Materials and Methods

Fly stocks and genetics

Fly stocks and crosses used in this study are listed in Supplemental Table S1. Crosses were maintained at 25°C. In the F1 generation, non-balancer females and males were used to set up cages that were incubated at 25°C. The F2 generation was used for imaging.

Live and fixed imaging

For live imaging, embryos were dechorionated in 50% bleach for 2 minutes, washed in water, and mounted onto a glass slide coated with embryo glue (double-sided tape dissolved in heptane). No. 1.5 coverslips coated in glue were attached to the slide to use as spacers and a No. 1 coverslip was attached on top to create a chamber. Halocarbon 27 oil was used to fill the chamber. All imaging took place at 23-25°C.

For imaging fixed embryos, embryos were dechorionated in 50 % bleach (Chlorox) for 2 minutes, washed in water, and then fixed in 4% paraformaldehyde (Electron Microscopy Sciences) in 0.1 M phosphate buffer at pH 7.4 with 50% heptane (Alfa Aesar) for 30 min and manually devitellinized (TLR stains) or devitellinized by removing fixative, adding 50% methanol (Sigma Aldrich), and vortexing (Pins and Mud). Manually devitellinized embryos were stored in 0.01% Tween 20 in PBS (PBS-T and embryos devitellinized with 50% methanol were stored in 100% methanol at −4°C and rehydrated in PBS-T.

Embryos were washed in PBS-T, blocked with 10% BSA in PBS-T, and incubated with antibodies diluted in PBS-T. Embryos were incubated with primary antibodies at room temperature for 2 h. Antibodies used in this study are listed in Supplemental Table S1. Secondary antibodies used were conjugated with Alexa Fluor 488, 568, or 647 (Invitrogen) diluted at 1:500 in 5% BSA in PBS-T incubated overnight at 4°C. After antibody incubation, embryos were mounted onto glass slides using AquaPolymount (Polysciences).

All images were taken on a Zeiss LSM 710 confocal microscope with a 40×/1.2 Apochromat water objective lens, an argon-ion, 561-nm diode, 594-nm HeNe, 633 HeNe laser, and Zen software. The pinhole was set to 1 airy unit (au) for fixed imaging and 2.5 au for live imaging. For two-color live imaging, band-pass filters were set at ~490–565 nm for GFP and ~590–690 nm for mCherry (mCh). For three-color imaging, band-pass filters were set at ~480–560 nm for Alexa Fluor 488, ~580–635 nm for Alexa Fluor 568, and ~660–750 nm for Alexa Fluor 647.

dsRNA injections

Primers included the sequence of the T7 promoter (TAATACGACTCACTATAGGGAGACCAC) followed by the following recognition sequences:
Toll 2 F: AGTTTGAATCGAAACGCGAG
Toll 2 R: GGACACTGCACCGGATGT
Toll 6 F: ATCGGCCAAAAAGAGCAGTA
Toll 6 R: AGCAGCGTGTGCAGATTATT
Toll 8 F: ATGCGTACCATTTTCCTACCA
Toll 8 R: TTTTTACTCTTCGCTTTTTCGC
Snα–F: CGGAACCGAAACGTGACTAT
Snα–R: GCGGTAGTTTTTGGCATGAT

Primer pairs were used to amplify a PCR product from genomic DNA. PCR products were directly used in a transcription reaction with T7 polymerase using the MEGAscript transcription kit (Ambion). The reaction was placed in boiling water and allowed to cool to room temperature to

782 promote annealing. RNA was extracted with phenol:chloroform, washed with ethanol, and
783 resuspended in 0.1M TE buffer.

784 Stage 2 embryos were dechorionated in 50% bleach for 2 minutes. The embryos were mounted
785 onto glass slides and desiccated for 4 min using Drierite. Embryos were covered with a 3:1 mixture
786 of halocarbon 700/halocarbon 27 oils and then injected laterally. Embryos were imaged 3 hours
787 after injecting.
788
789 **Drug injections**
790 Embryos were dechorionated in 50% bleach for 2 minutes. The embryos were mounted onto
791 glass slides and desiccated for 4 min using Drierite. Embryos were covered with a 3:1 mixture of
792 halocarbon 700/halocarbon 27 oils and then injected laterally at the beginning of cephalic furrow
793 formation. To disrupt F-actin we resuspended CtyoD (Enzo Life Sciences) at 0.125 mg/ml in
794 DMSO. Embryos were imaged 3-5 minutes after injecting.
795
796 **Laser ablation**
797 Laser ablations were performed using a 2-photon Mai-Tai laser set to 800 nm on a LSM710
798 confocal microscope (Zeiss) through a 40x/1.1 objective, using the Zen software (Zeiss) (W. M.
799 Keck Microscopy Facility, Cambridge, MA). For ablations, laser power was set at 20%, with a
800 scan speed of 1.58 ms/px. Ablations were performed with four overlapping linear ROIs around
801 one side of MD1.
802 Sham ablations were performed with the same setup as the laser ablations except the laser power
803 was set at 10%. This caused the ROIs to become bleached, but not ablated.
804
805 **Image processing and analysis**
806 All figure images were processed using MATLAB (MathWorks) and FIJI
807 (http://fiji.sc/wiki/index.php/Fiji). A Gaussian smoothing filter (kernel = 0.75 pixel) was applied to
808 all figure images. Brightness and contrast were adjusted to optimally visualize the mitotic spindle
809 or Pins crescents in figure images. Control and experimental images were adjusted the same.
810
811 *Division angle analysis*
812 Division angle was taken using the angle tool in FIJI and measured as the angle between spindle
813 poles axis and the AP axis in mitotic cells at anaphase or later. The angle values range from 0
814 degrees, indicating alignment along AP, to 90 degrees, indicating alignment along DV. Unless
815 otherwise stated, 10 embryos and between 100-250 spindles were counted of each genotype.
816 Resulting angles were plotted in rose plots, with percentage of spindles on the r axis and angle
817 on the theta axis.
818
819 *Intensity profile analysis*
820 Intensity profiles were taken using the segmented line tool in Fiji with a line width of 2 and
821 measured using the Plot Profile feature in Fiji. The perimeter of the cell was outlined starting at
822 the apical most point of mitotic cells in anaphase. The direction of the lines was toward the dorsal
823 midline or ventral midline (clockwise for the left half of the domains and counterclockwise for the
824 right half of the domains). Intensity was normalized to cytoplasmic intensity, which was measured
825 as the mean grey value of a line drawn through the cytoplasm. Unless otherwise stated, 10 cells
826 per embryo and 3 embryos per genotype were analyzed, averaged, and graphed as line plots
827 with normalized intensity on the y axis and distance from start on the x axis.
828
829 *Anisotropy analysis*
830 Aspect ratios of interphase cells were taken using the polygon tool in Fiji and the Fit Ellipse
831 measurement, which gives the major axis length, the minor axis, and the angle of the major axis.

Aspect ratio is ratio between the major axis and the minor axis. The average aspect ratio was recorded and the angle of the major axis was compared to the axis of division. Unless otherwise stated, 10 cells per embryo and 3 embryos per genotype were analyzed.

Quantification and statistical analysis

Statistical analyses were performed using the MATLAB statistics toolbox. p values were calculated using a two-sample Mann-Whitney test, the reference sample is the angle distribution in wild-type. Correlation coefficients r are Spearman correlation coefficient. p values are calculated against the null hypothesis r = 0.

Figure Legends

Figure 1. Early mitotic domains in the *Drosophila* head exhibit spindle rotation and oriented division (A) Schematic of the dorsal head of a *Drosophila* embryo with mitotic domain 1 (MD1) in red, mitotic domain 3 (MD3) in blue, and mitotic domain 5 (MD5) in orange. Anterior-posterior (AP) axis is indicated by arrow, the top of images will consistently be anterior, as in the schematic. (B) Image of the dorsal head of a live *Drosophila* embryo expressing Jupiter::GFP to label microtubules/spindle (greyscale). Jupiter::GFP signal is detected in image. MD1 is outlined in red, MD3 in blue, and MD5 in orange, scalebar is 50 µm. (C) MD1 cells exhibit planar polarized cell division. Left, Image of MD1 in live embryo showing labeled myosin (greyscale, Sqh::mCherry), to show cytokinetic rings, and labeled F-actin (green, UtrABD::GFP) to show cell cortex, scalebar is 10 µm. Right, Same image of MD1 annotated with black lines marking the cytokinetic ring of each dividing cell and magenta dashed lines marking division angle. (D) MD1 cells exhibit spindle rotation and alignment. Images are time series of MD1 with Jupiter::GFP marking the mitotic spindle (greyscale), blue lines indicate spindles still rotating and magenta lines represent spindle that have reached their final orientation, scalebar is 10 µm. (E) Schematic of division angle analysis. Division angle is taken with respect to the AP axis such that angle of 0 indicates alignment with the AP axis. Note only spindles during or after anaphase, when division angle is fixed, are measured. (F-H) Rose plots indicating division angles of MD1 (F), MD3 (G), and MD5 (H). Red lines indicate mean division angle. Mean division angle for MD=21.6°, MD3=20.4°, and MD5=19.0°. For MD1, n=10 embryos and 200 spindles, MD3, n=5, embryos and 123 spindles and MD5, n=5 embryos and 140 spindles.

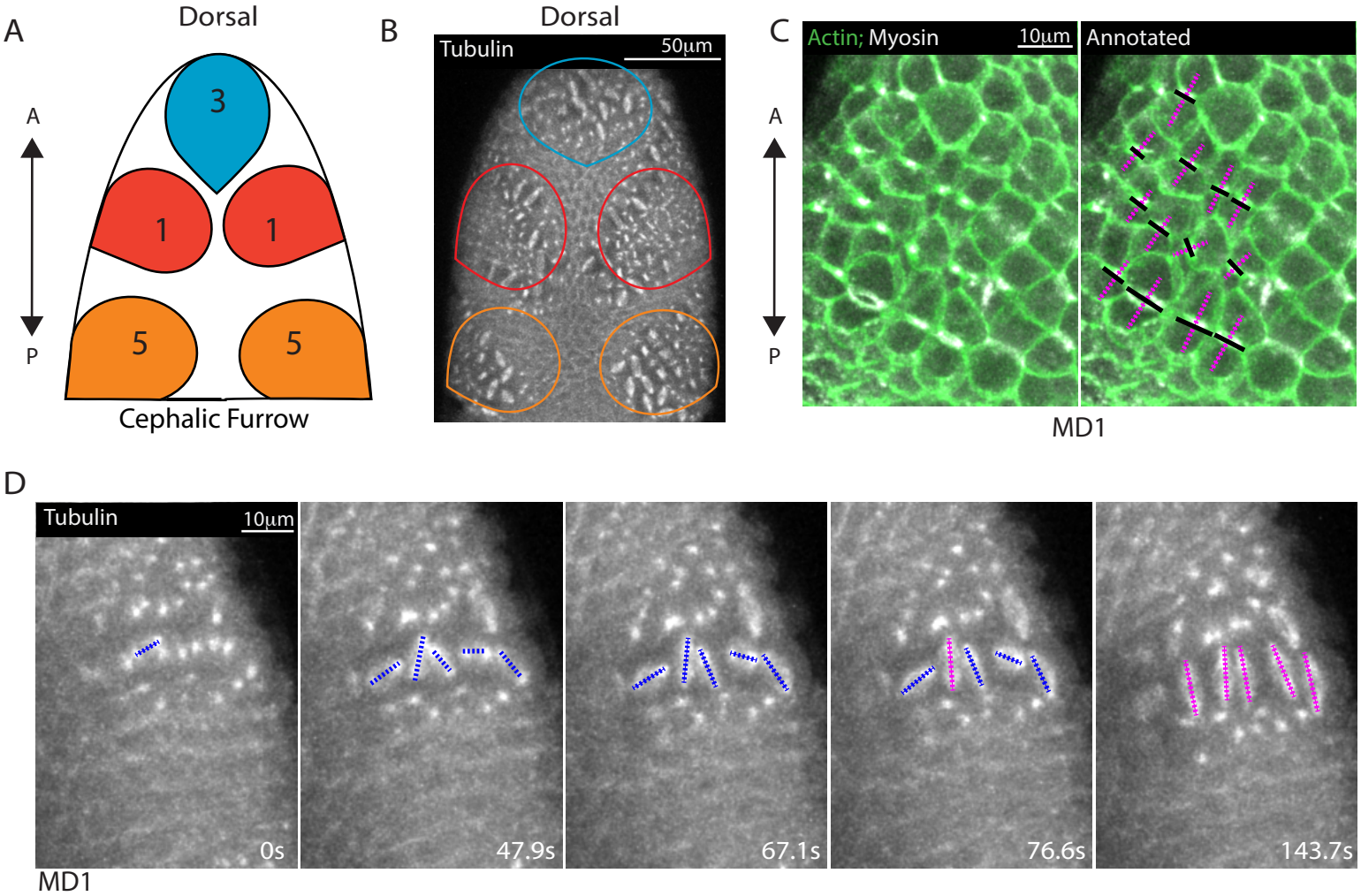
A
Dorsal
A
P
3
1
1
5
5
Cephalic Furrow
B
Dorsal
Tubulin
50µm
C
Actin; Myosin
10µm
Annotated
A
P
MD1
D
Tubulin
10µm
0s
47.9s
67.1s
76.6s
143.7s
MD1

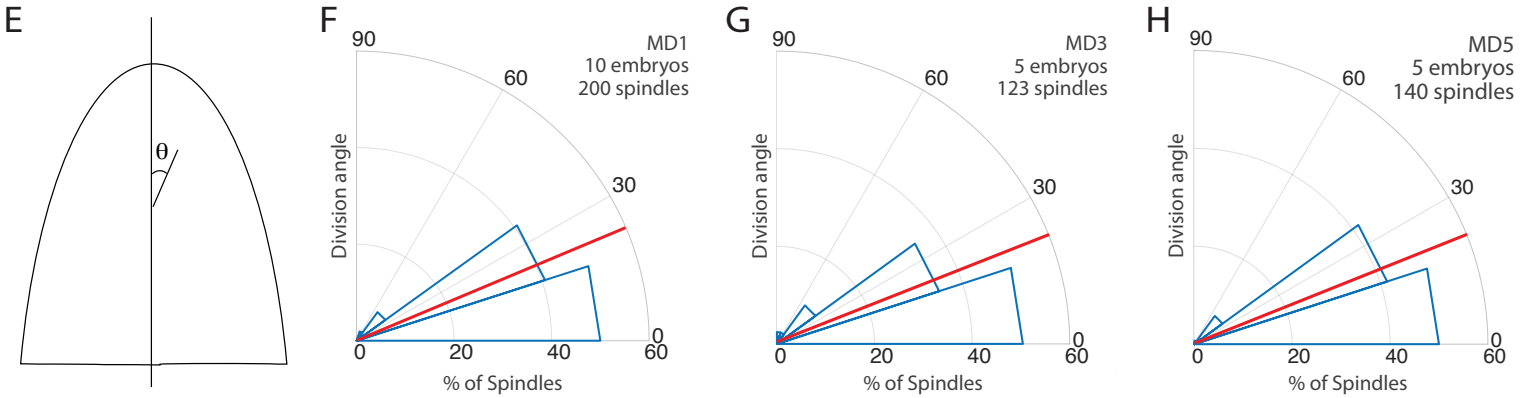
E
θ
F
MD1
10 embryos
200 spindles
Division angle
% of Spindles
G
MD3
5 embryos
123 spindles
Division angle
% of Spindles
H
MD5
5 embryos
140 spindles
Division angle
% of Spindles

Figure 2. Pins is planar polarized in mitotic domain cells. (A-B) Time series of MD1 of embryo expressing Pins::YFP, to label spindle rotation machinery, and Gap43::mCherry, to mark membranes. scalebar is 10 µm. (C, J) Quantification of average cellular (7-9 cells) Pins::YFP signal intensity around the mitotic cell cortex for 3 separate embryos, lines indicate average of cells in each embryo for MD1 (C) or MD14 (J). Cortical intensity was measured at anaphase, indicated by cell elongation, and normalized to cytoplasmic Pins::YFP signal. (C', J') Average of embryos in C or J. (D, K) Quantification of Gap43::mCherry (membrane marker) intensity for same cells and 3 embryos as in C for MD1 or J for MD14. (D', K') Average of embryos in D, MD1, or K, MD14. Intensity was normalized to cytoplasmic Gap43::mCherry signal. (E) Fixed sample of metaphase cells in MD1 stained for Tubulin (Left), Ecadherin (center), and Pins (Right). (F) Fixed sample of anaphase cells in MD1 stained for Tubulin (Left), Pins (Right). (G) Fixed sample of anaphase cells in MD1 stained for Tubulin (Left) and Mud (Right). (H-I) Time series of MD14 cells expressing Pins::YFP and Gap43::mCherry, similar to A and B. scalebar is 10 µm.

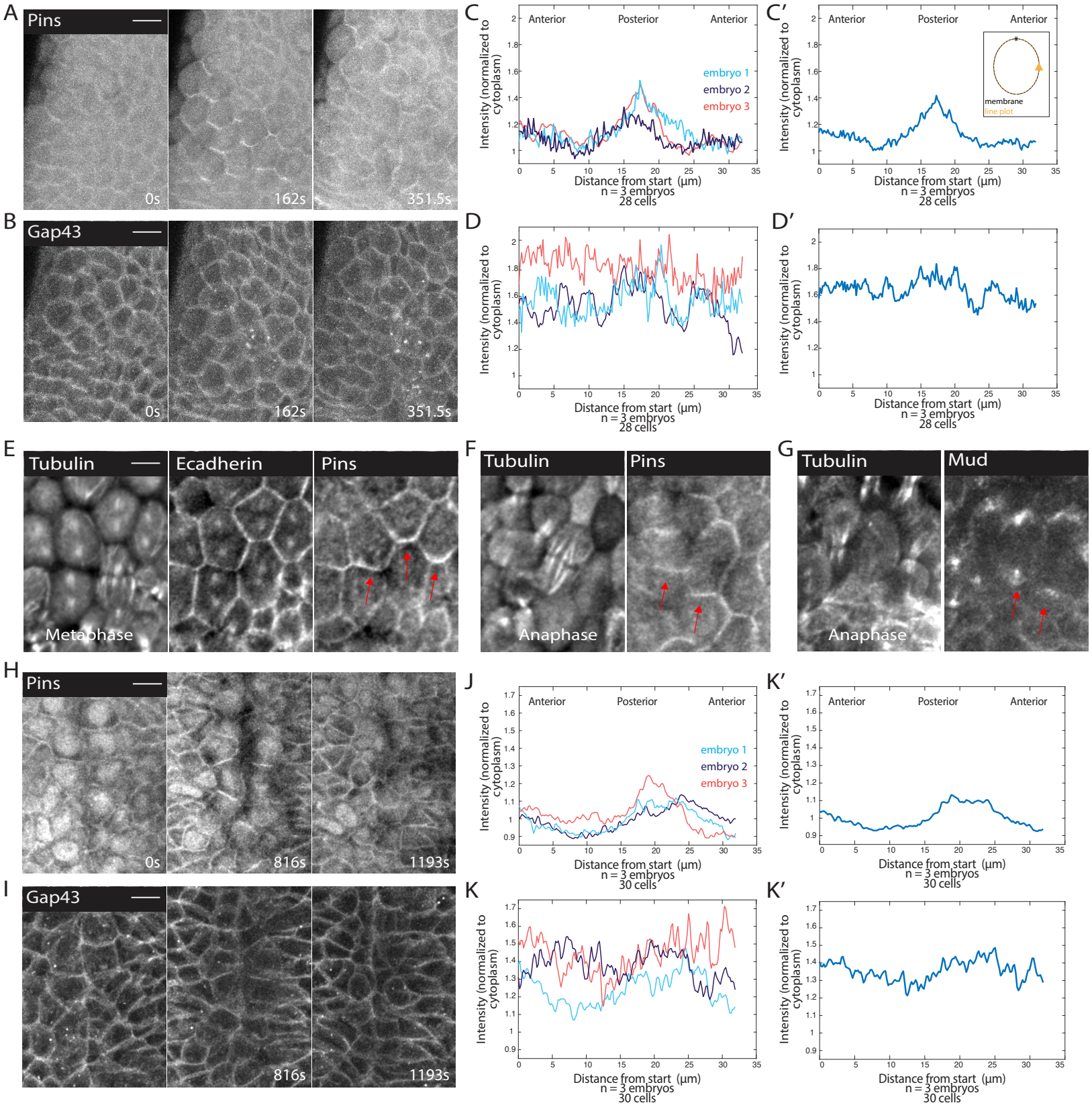
A
Pins
0s
162s
351.5s
B
Gap43
0s
162s
351.5s
C
Anterior
Posterior
Anterior
embryo 1
embryo 2
embryo 3
Intensity (normalized to cytoplasm)
Distance from start (µm)
n = 3 embryos
28 cells
C′
Anterior
Posterior
Anterior
membrane
line plot
Intensity (normalized to cytoplasm)
Distance from start (µm)
n = 3 embryos
28 cells
D
Intensity (normalized to cytoplasm)
Distance from start (µm)
n = 3 embryos
28 cells
D′
Intensity (normalized to cytoplasm)
Distance from start (µm)
n = 3 embryos
28 cells
E
Tubulin
Ecadherin
Pins
Metaphase
F
Tubulin
Pins
Anaphase
G
Tubulin
Mud
Anaphase
H
Pins
0s
816s
1193s
I
Gap43
816s
1193s
J
Anterior
Posterior
Anterior
embryo 1
embryo 2
embryo 3
Intensity (normalized to cytoplasm)
Distance from start (µm)
n = 3 embryos
30 cells
K′
Anterior
Posterior
Anterior
Intensity (normalized to cytoplasm)
Distance from start (µm)
n = 3 embryos
30 cells
K
Intensity (normalized to cytoplasm)
Distance from start (µm)
n = 3 embryos
30 cells
K′
Intensity (normalized to cytoplasm)
Distance from start (µm)
n = 3 embryos
30 cells

Figure 3. Planar polarized divisions depend on asymmetric Pins localization (A–B) Pins localizes in planar polarized crescents immediately prior to spindle orientation. Images are time series of MD1 of embryo with labeled Pins (Pins::YFP) and labeled tubulin (Tubulin::mCherry), to mark mitotic spindles, blue lines indicate spindles that are still rotating, magenta lines indicate spindles that have reached their final orientation. Colored boxes at tips of lines label spindles with the color marking the same spindle at each time point. Scalebar is 10 µm. (C) Spindle orientation is correlated with Pins polarity. Plot of the correlation between the angle of maximum Pins::YFP intensity and division angle., R^2=0.77. (D) Schematic of MD 14, located on either side of the ventral midline. (E-F) Images are a time series of MD14 cells labeled with Pins::YFP and tubulin::mCherry, to mark mitotic spindles. (G, I) Myristoylated Pins disrupts division orientation. Left, image of MD1 of control embryo (G, UAS>PinsGFP) or MD1 of Myristoylated Pins expressing embryo (I, UAS>myr::Pins::GFP). Images show marker (CLIP170::GFP) to mark mitotic spindles (greyscale), scalebar is 10 µm. Right, same image annotated with dashed lines to indicate spindle position. (H, J) Quantification of spindle angles for control embryos (H, UAS>PinsGFP) using rose plots or Myristoylated Pins expressing embryos (J, UAS>myr::Pins::GFP). For control embryos (H, UAS-PinsGFP) MD1, n=7 embryos and 175 spindles. For Myristoylated Pins expressing embryos, n=10 embryos and 284 spindles. Average orientation angles per embryo were statistically different between control and Myristoylated Pins expressing embryos, KS test, p=0.0326. (K, M) Pins asymmetry is required for MD14 spindle orientation. Left, image of MD14 of control embryo (G, UAS-PinsGFP) or MD14 of Myristoylated Pins expressing embryo (I, UAS>myr::Pins::GFP). Images show marker (CLIP170::GFP) to mark mitotic spindles (greyscale), scalebar is 10 µm. Right, same image annotated with dashed lines to indicate spindle position. (L, N) Quantification of spindle angles for control embryos (UAS>PinsGFP) or Myristoylated Pins expressing embryos (N, UAS>myr::Pins::GFP) using rose plots. For control embryos (L, UAS>PinsGFP) MD14, n=3 embryos and 64 spindles. For Myristoylated Pins expressing embryos, n=3 embryos and 59 spindles. Average orientation angles per embryo were statistically different between control and Myristoylated Pins expressing embryos, KS test, p=0.0326.

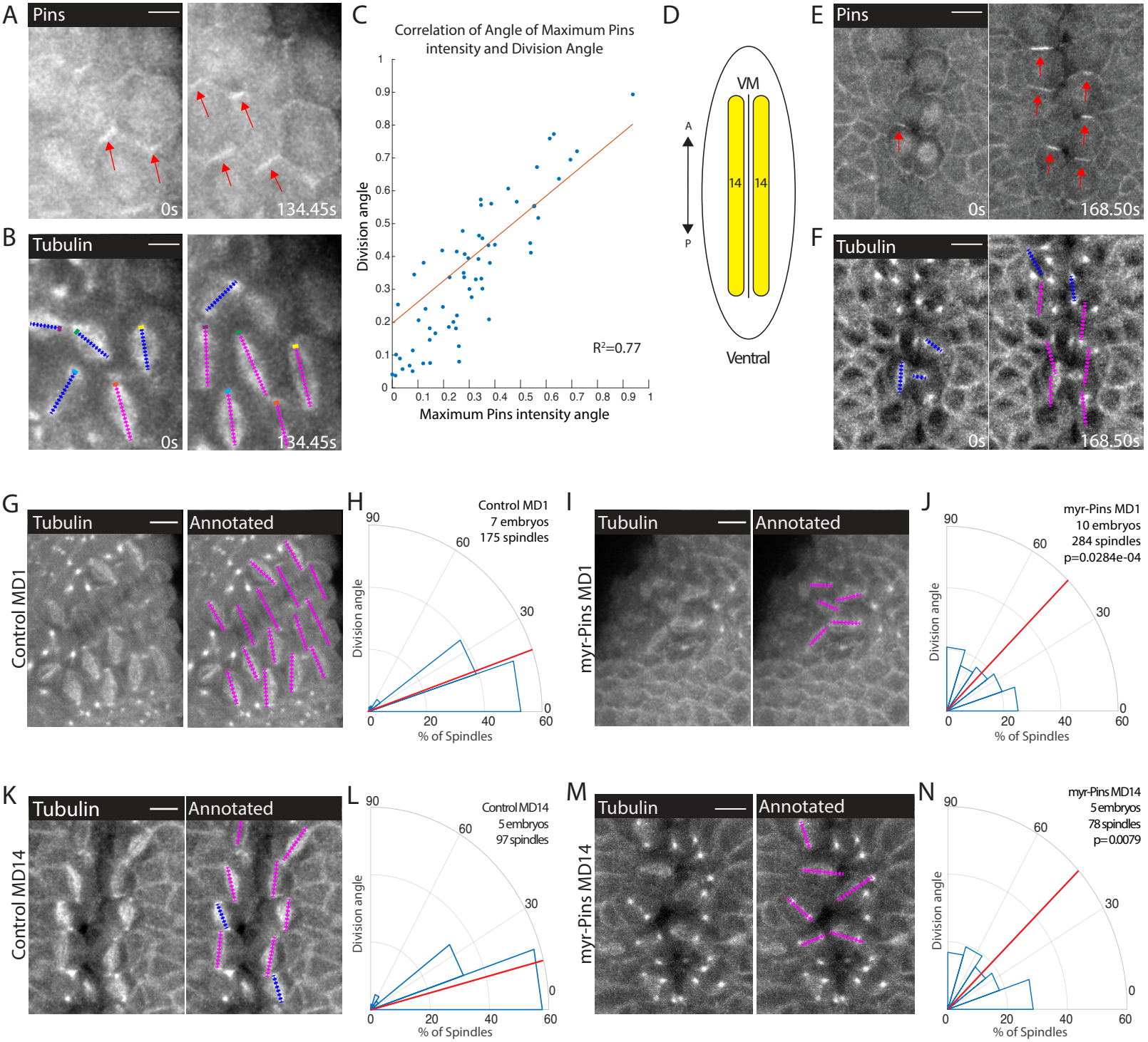
A
Pins
0s
134.45s
B
Tubulin
0s
134.45s
C
Correlation of Angle of Maximum Pins intensity and Division Angle
Division angle
Maximum Pins intensity angle
R²=0.77
D
VM
A
P
14
14
Ventral
E
Pins
0s
168.50s
F
Tubulin
0s
168.50s
G
Tubulin
Annotated
Control MD1
H
Control MD1
7 embryos
175 spindles
Division angle
% of Spindles
I
Tubulin
Annotated
myr-Pins MD1
J
myr-Pins MD1
10 embryos
284 spindles
p=0.0284e-04
Division angle
% of Spindles
K
Tubulin
Annotated
Control MD14
L
Control MD14
5 embryos
97 spindles
Division angle
% of Spindles
M
Tubulin
Annotated
myr-Pins MD14
N
myr-Pins MD14
5 embryos
78 spindles
p=0.0079
Division angle
% of Spindles

Figure 4. Disruption of adherens junctions, but not Canoe, inhibits planar polarized division orientation (A, C, E) α–catenin depletion disrupts division orientation. Left, image of MD1 of control knock-down (A, Rh3 RNAi), MD1 of α–catenin depleted embryo (C, α–catenin RNAi), or MD1 of Canoe depleted embryo (E, Canoe RNAi). Images show marker (CLIP170::GFP) to mark mitotic spindles (greyscale), scalebar is 10 µm. Right, same image annotated with dashed lines to indicate spindle position. (B, D, F) Quantification of spindle angles for control embryos (B, Rh3 RNAi), α–catenin depleted embryos (D, α–catenin RNAi), or Canoe depleted embryos (F, Canoe RNAi) using rose plots. For control embryos (Rh3 RNAi) MD1, n=10 embryos and 355 spindles. For α–catenin RNAi MD1, n=10 embryos and 248 spindles. For Canoe RNAi MD1, n=7 embryos and 166 spindles. Average orientation angles per embryo were statistically different between control and α–catenin RNAi, p=0.0012, but not for canoe RNAi, p=0.2698.

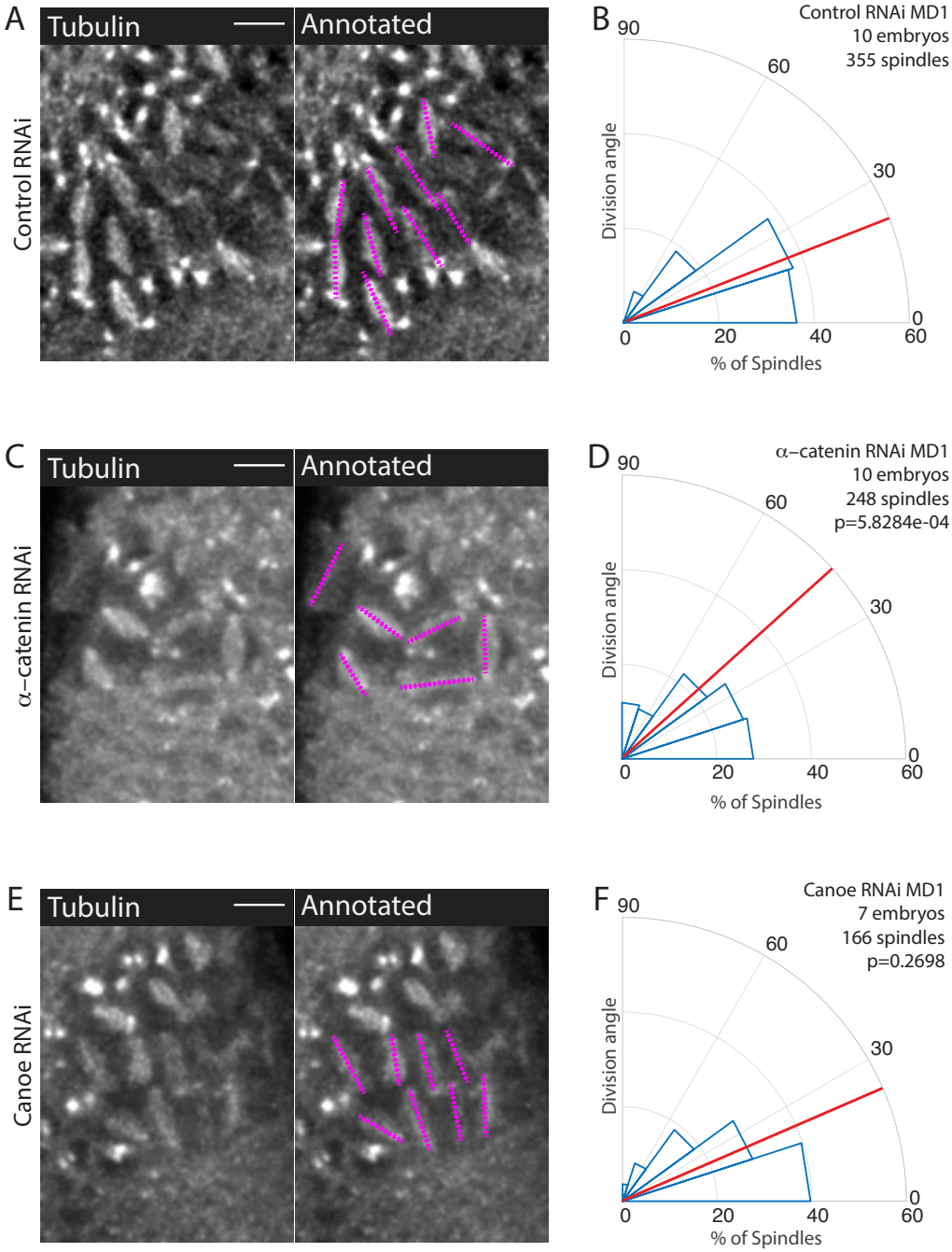
A
Tubulin
Annotated
Control RNAi
B
Control RNAi MD1
10 embryos
355 spindles
Division angle
% of Spindles
C
Tubulin
Annotated
α−catenin RNAi
D
α−catenin RNAi MD1
10 embryos
248 spindles
p=5.8284e-04
Division angle
% of Spindles
E
Tubulin
Annotated
Canoe RNAi
F
Canoe RNAi MD1
7 embryos
166 spindles
p=0.2698
Division angle
% of Spindles

Figure 5. Adherens junction depletion disrupts Pins planar cell polarity. (A, C) α–catenin depletion disrupts Pins localization. Left, image of a MD1 cell of control embryo (A, Rh3 RNAi) or a MD1 cell of α–catenin depleted embryo (C, α–catenin RNAi). Images show labelled Pins (Pins::YFP), scalebar is 10 μm. Right, same image annotated with dashed line to indicate cell outline used to plot intensity profile, * to indicate start, and arrow to indicate direction of line. (B, D) Quantification of Pins intensity for control embryos (Rh3 RNAi) or α–catenin depleted embryos (D, α–catenin RNAi). Intensity was normalized to cytoplasm. For control (Rh3) MD1, n=3 embryos and 30 cells. For α–catenin RNAi MD1, n=3 and 30 cells.

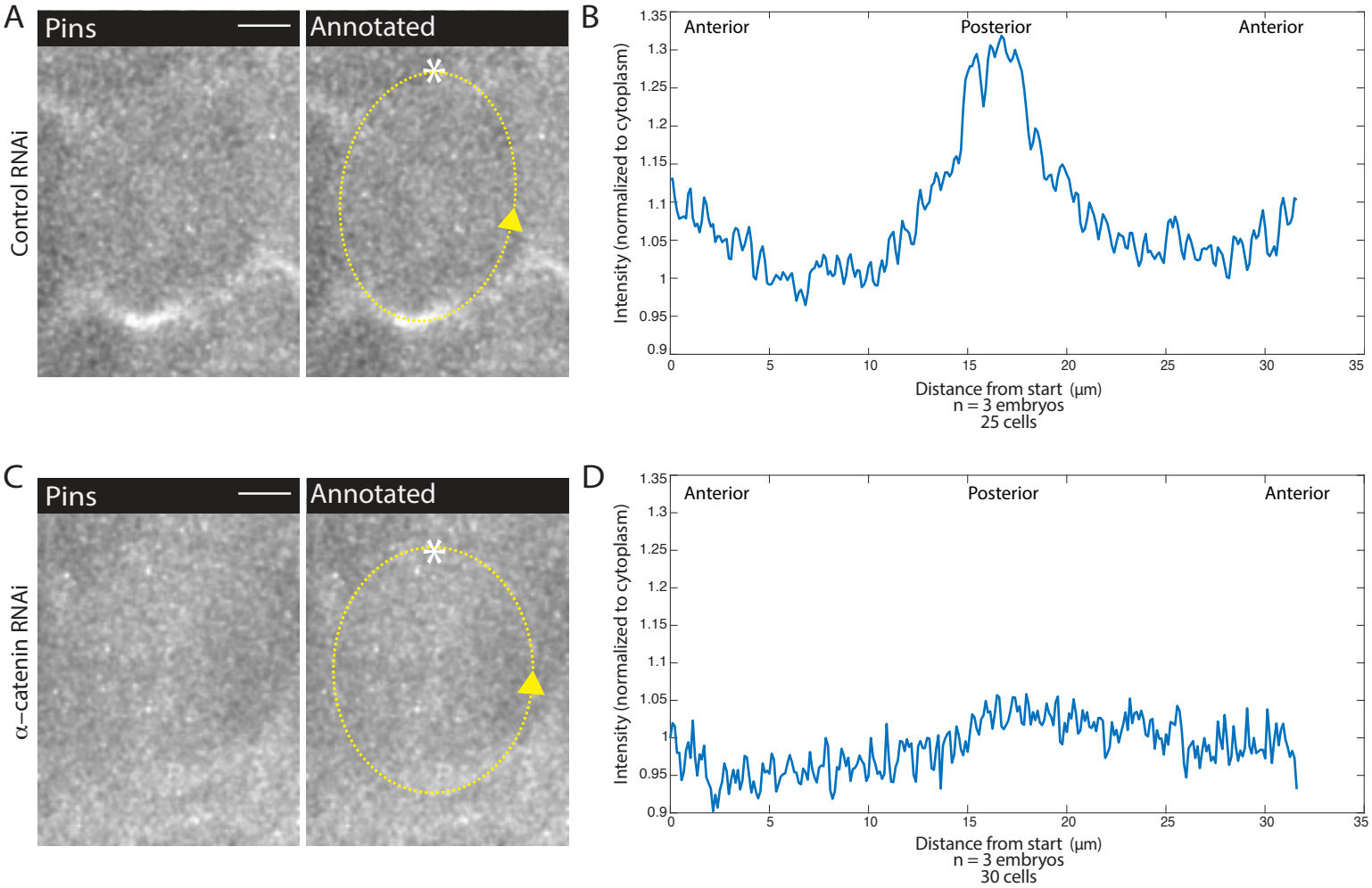
A
Pins
Annotated
Control RNAi
B
Anterior
Posterior
Anterior
Intensity (normalized to cytoplasm)
Distance from start (μm)
n = 3 embryos
25 cells
C
Pins
Annotated
α−catenin RNAi
D
Anterior
Posterior
Anterior
Intensity (normalized to cytoplasm)
Distance from start (μm)
n = 3 embryos
30 cells

Figure 6. Mechanical force is necessary for Pins polarity and spindle orientation (A, E) Cytoskeletal disruption prevents Pins localization. Image of MD1 in control embryo (A, DMSO injection) or MD1 of cytochalasin D (CytoD) injected embryo (E, 0.25mg/mL CytoD injection). Images show labelled Pins (Pins::YFP), red arrows point to crescents of Pins in control MD1, scalebar is 10 µm. (B, F) Cytoskeletal disruption interferes with division orientation. Image of MD1 of control embryo, same embryo as A, (B, DMSO injection) or MD1 of CytoD injected embryo (F). Images, from same embryo as E, show marker (Tubulin::mCherry) to mark mitotic spindles (greyscale), scalebar is 10 µm. Right, same image annotated with dashed lines to indicate spindle position. (C, G) Quantification of Pins intensity for control embryos (C, DMSO injection) or CytoD injected embryo (G, 0.25mg/mL CytoD injection). Intensity was normalized to cytoplasm. For control (DMSO injection) MD1, n=3 embryos and 30 cells. For CytoD injection MD1, n=3 and 28 cells. (D, H) Quantification of spindle angles for control embryos (H, DMSO injection) or CytoD injected embryo (H) using rose plots. For control embryos (DMSO injection) MD1, n=5 embryos and 162 spindles. For CytoD injection MD1, n=6 embryos and 143 spindles. When compared to control (DMSO injection) using KS test, p=0.0023. (I) Schematic of laser ablation schema. The ROI for laser cutting was drawn around MD1 on one side of the embryo to mechanically uncouple MD1 from surrounding tissue. The other side of MD1 was not cut. (J-L) Separating MD1 from surrounding tissue disrupts spindle orientation. Left, image of MD1 on control side of embryo (J, non-cut), laser cut side of embryo (K), or sham ablation, control embryos (L). Images show marker (Tubulin::mCherry) to mark mitotic spindles (greyscale), scalebar is 10 µm. Right, same image annotated with dashed lines to indicate spindle position, red box indicates laser cut ROI. (M-O) Quantification of spindle angles for control side (M, non-cut), laser cut side (N), or MD1 of sham ablated embryos (O) using rose plots. For control side (non-cut) MD1, n=2 embryos and 15 spindles. For laser cut side MD1, n=4 embryos and 56 spindles. For sham ablated embryos MD1, n-4 embryos and 58 spindles. Average orientation angles per embryo were statistically different between laser cut and non-cut sides of MD1, p=0.0469, and between laser cut embryos and sham ablation embryos, p=0.0111.

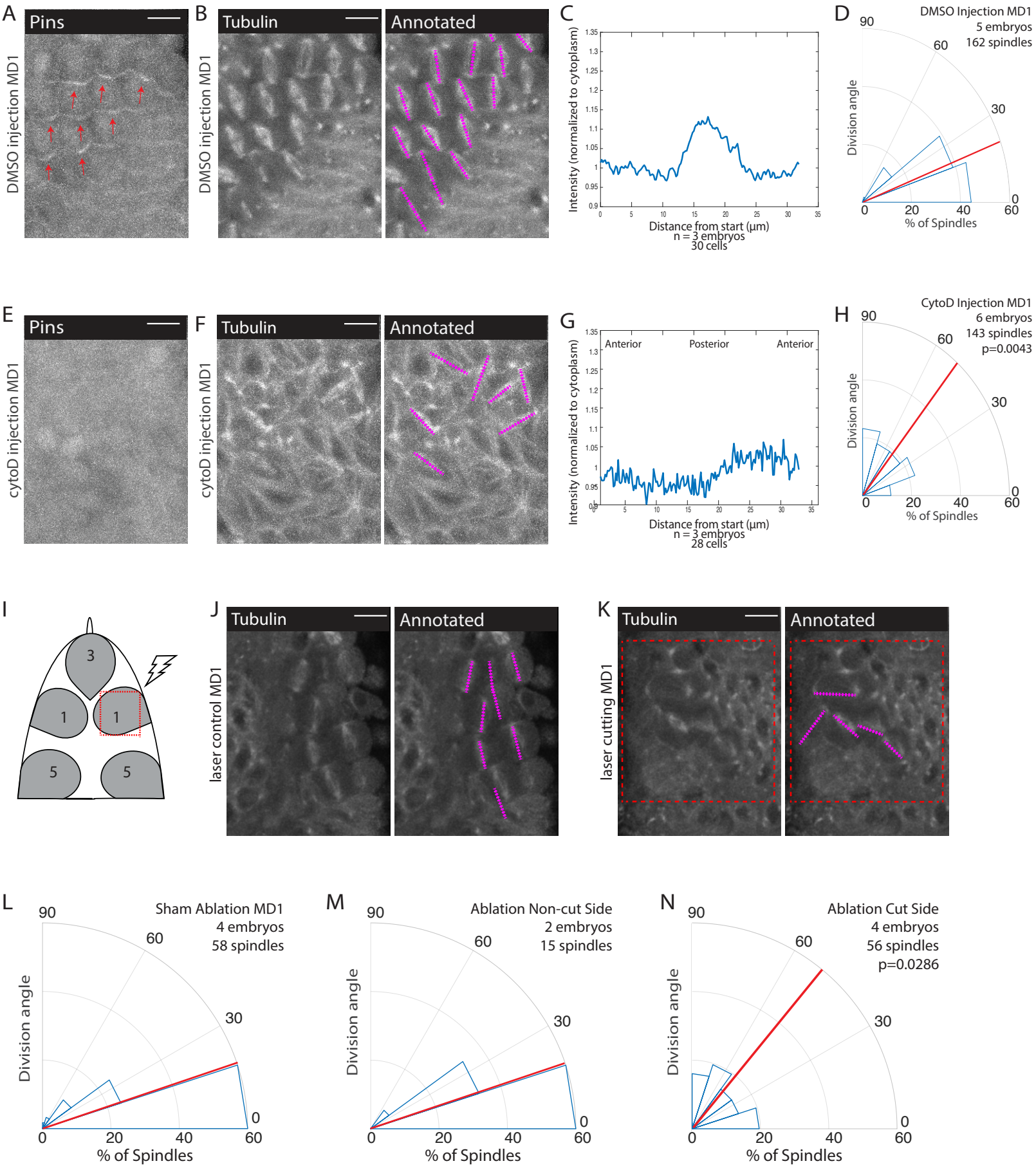
A
Pins
DMSO injection MD1
B
Tubulin
Annotated
DMSO injection MD1
C
Intensity (normalized to cytoplasm)
Distance from start (µm)
n = 3 embryos
30 cells
D
DMSO Injection MD1
5 embryos
162 spindles
Division angle
% of Spindles
E
Pins
cytoD injection MD1
F
Tubulin
Annotated
cytoD injection MD1
G
Anterior
Posterior
Anterior
Intensity (normalized to cytoplasm)
Distance from start (µm)
n = 3 embryos
28 cells
H
CytoD Injection MD1
6 embryos
143 spindles
p=0.0043
Division angle
% of Spindles
I
3
1
1
5
5
J
Tubulin
Annotated
laser control MD1
K
Tubulin
Annotated
laser cutting MD1
L
Sham Ablation MD1
4 embryos
58 spindles
Division angle
% of Spindles
M
Ablation Non-cut Side
2 embryos
15 spindles
Division angle
% of Spindles
N
Ablation Cut Side
4 embryos
56 spindles
p=0.0286
Division angle
% of Spindles

1184 **Figure 7. Snail depletion disrupts Pins polarization and spindle orientation** (A, E) Disrupting
1185 ventral furrow formation disrupts Pins polarity. Image of MD1 of control embryo (A, 0.1x TE buffer
1186 injection) or MD1 of Snail dsRNA injected embryo (E). Images show labelled Pins (Pins::YFP),
1187 red arrows point to crescents of Pins in control, scalebar is 10 µm. (B, F) Snail depletion disrupts
1188 division orientation. Left, image of MD1 of control embryo (B, 0.1x TE buffer injection) or MD1 of
1189 Snail depleted embryo (F). Images show marker (Tubulin::mCherry) to mark mitotic spindles
1190 (greyscale), scalebar is 10 µm. Right, same image annotated with dashed lines to indicate spindle
1191 position. (C, G) Quantification of Pins intensity for control embryos (C, 0.1x TE buffer injection) or
1192 Snail dsRNA injected embryo (G). Intensity was normalized to cytoplasm. For control (0.1x TE
1193 buffer injection) MD1, n=3 embryos and 30 cells. For Snail depletion MD1, n=2 and 20 cells. (D,
1194 H) Quantification of spindle angles for control embryos (H, 0.1x TE buffer injection) or Snail
1195 dsRNA injected embryo (H) using rose plots. For control embryos (0.1x TE buffer injection) MD1,
1196 n=6 embryos and 166 spindles. For Snail dsRNA injection MD1, n=2 embryos and 23 spindles.
1197 Average orientation angles per embryo were statistically different between control and Snail
1198 dsRNA injected embryos, KS test, p=0.0326.

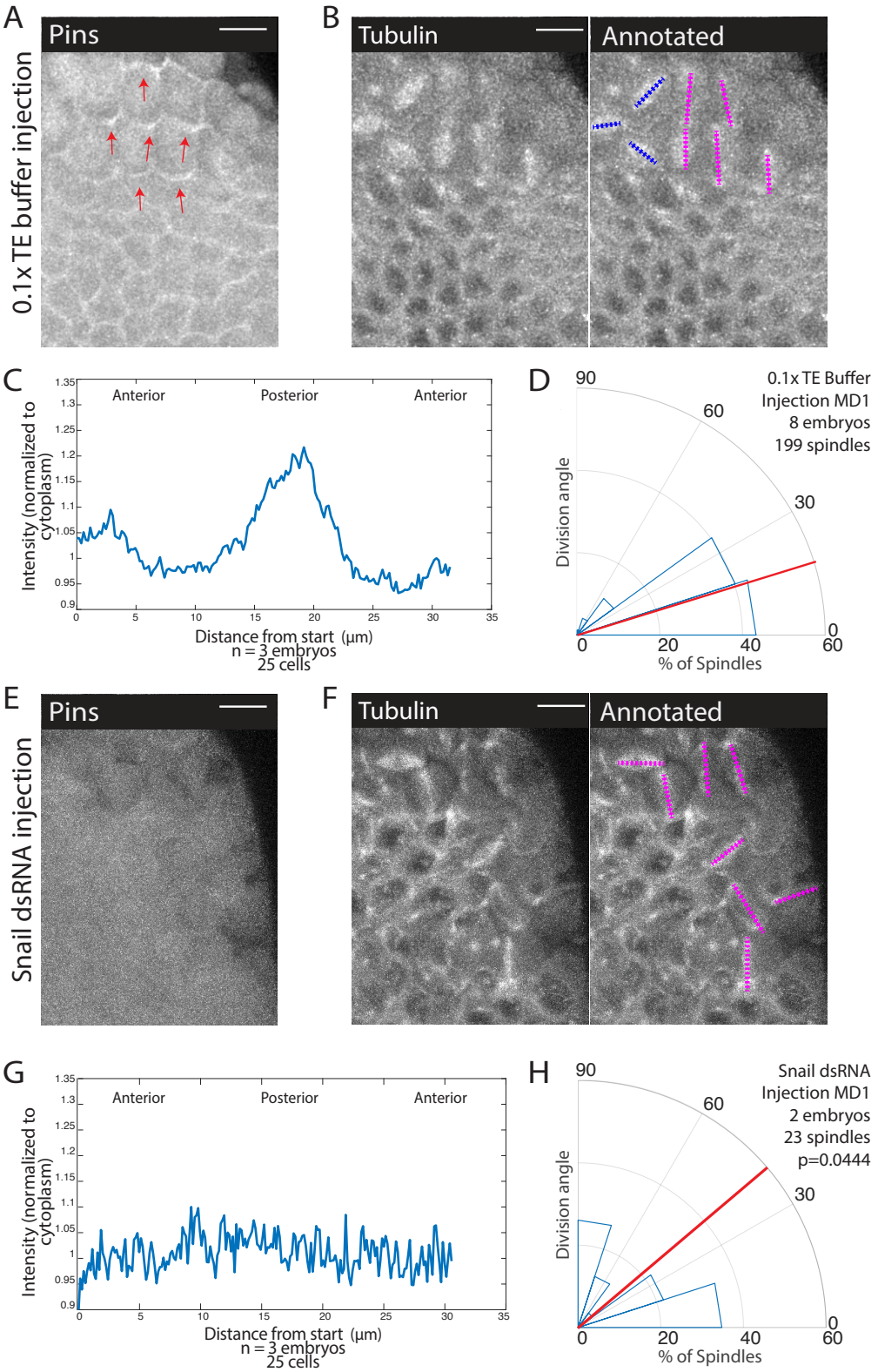
A
Pins
0.1x TE buffer injection
B
Tubulin
Annotated
C
Anterior
Posterior
Anterior
Intensity (normalized to cytoplasm)
Distance from start (µm)
n = 3 embryos
25 cells
D
0.1x TE Buffer
Injection MD1
8 embryos
199 spindles
Division angle
% of Spindles
E
Pins
Snail dsRNA injection
F
Tubulin
Annotated
G
Anterior
Posterior
Anterior
Intensity (normalized to cytoplasm)
Distance from start (µm)
n = 3 embryos
25 cells
H
Snail dsRNA
Injection MD1
2 embryos
23 spindles
p=0.0444
Division angle
% of Spindles